

Modified second-order generalized integrators with modified frequency locked loop for fast harmonics estimation of distorted single-phase signals (LONG VERSION)

C.M. Hackl^{‡,*} and M. Landerer[†]

Abstract

This paper proposes *modified Second-Order Generalized Integrators* (mSOGIs) for a fast estimation of all harmonic components of arbitrarily distorted single-phase signals such as voltages or currents in power systems. The estimation is based on the internal model principle leading to an overall observer system consisting of parallelized mSOGIs. The observer is tuned by pole placement. For a constant fundamental frequency, the observer is capable of estimating all harmonic components with prescribed settling time by choosing the observer poles appropriately. For time-varying fundamental frequencies, the harmonic estimation is combined with a *modified Frequency Locked Loop* (mFLL) with gain normalization, sign-correct anti-windup and rate limitation. The estimation performances of the proposed parallelized mSOGIs with and without mFLL are illustrated and validated by measurement results. The results are compared to standard approaches such as parallelized standard SOGIs (sSOGIs) and adaptive notch filters (ANFs).

Index Terms

Second-Order Generalized Integrator, Frequency Locked Loop, amplitude estimation, phase estimation, frequency estimation,

***A shorter version of this paper has been submitted to and accepted for publication in *IEEE Transactions on Power Electronics* (DOI: 10.1109/TPEL.2019.2932790; for more details see [1]) ***
This long version includes (i) more detailed explanations, (ii) more simulation and measurement results and (iii) a thorough theoretical analysis in its Appendix.

CONTENTS

I	Introduction	2
I-A	Motivation and literature review	2
I-B	Problem statement	4
I-C	Principle idea of proposed solution	4
II	Second-Order Generalized Integrators (SOGIs): In-phase and quadrature signal estimation	5
II-A	Standard SOGI (sSOGI) for the ν -th harmonic component	5
II-B	Modified SOGI (mSOGI) for the ν -th harmonic component	6
II-C	Comparison of the estimation performances of sSOGI and mSOGI	7
II-D	Parallelization of the mSOGIs	8
III	Frequency-Locked Loop (FLL): Frequency estimation	9
III-A	Standard FLL (sFLL)	9
III-A1	Adaption law	10
III-A2	Gain Normalization (GN)	10
III-B	Modified FLL (mFLL)	10
III-B1	Generalized adaption law	11
III-B2	Sign-correct anti-windup strategy	11
III-B3	Rate limitation	12
III-C	Generalized adaption law	12

[‡]C.M. Hackl is with the Munich University of Applied Sciences (MUAS) and head of the “Control of Renewable Energy Systems (CRES)” research group at Technical University of Munich (TUM), Germany (e-mail: christoph.hackl@hm.edu).

[†]M. Landerer is with the research group “Control of renewable energy systems” (CRES) at the Munich School of Engineering (MSE), Technical University of Munich (TUM), Germany (e-mail: markus.landerer@tum.de).

* Authors are in alphabetical order and contributed equally to the paper. Corresponding author is C.M. Hackl (christoph.hackl@hm.edu).

IV	Implementation and measurement results	12
IV-A	Discussion of the measurement results obtained for Scenario (S_1)	14
IV-B	Discussion of the measurement results obtained for Scenario (S_2)	14
V	Conclusion	18
Appendix		21
A	Recapitulation	21
B	Observability of the parallelized internal models (27) (for constant $\hat{\omega}$)	21
C	Bounded-input bounded-state/bounded-output stability of the nonlinear observer	21
D	Boundedness and exponential decay of the signal estimation error	22
E	Pole placement algorithm for the parallelized mSOGIs	24
F	Generalization of the adaption law of the mFLL for the parallelized mSOGIs	26
F1	Preliminaries	26
F2	Steady-state analysis (amplitude and phase responses) of parallelized mSOGIs	26
F3	Sign-correct adaption law	27
References		30

Notation

$\mathbb{N}, \mathbb{R}, \mathbb{C}, \mathbb{Q}$: natural, real, complex and rational numbers. For the following, let $n, m \in \mathbb{N}$. $\mathbf{x} := (x_1, \dots, x_n)^\top \in \mathbb{R}^n$: column vector (where $:=$ means “is defined as” and $^\top$ means “transposed”). $\mathbf{0}_n := (0, 0, \dots, 0)^\top \in \mathbb{R}^n$: zero vector. $\mathbf{1}_n := (1, 1, \dots, 1)^\top \in \mathbb{R}^n$: vector of ones. $\|\mathbf{x}\| := \sqrt{\mathbf{x}^\top \mathbf{x}}$: Euclidean norm of \mathbf{x} . $\mathbf{A} \in \mathbb{R}^{n \times m}$: real (non-square) matrix. $\text{diag}(\mathbf{a}) \in \mathbb{R}^{n \times n}$: diagonal matrix with diagonal entries taken from vector $\mathbf{a} = (a_1, \dots, a_n)^\top \in \mathbb{R}^n$. $\mathbf{O}_{n \times m} \in \mathbb{R}^{n \times m}$: zero (non-square) matrix. $\mathbf{I}_n := \text{diag}(\mathbf{1}_n) \in \mathbb{R}^{n \times n}$: identity matrix. $\text{blockdiag}(\mathbf{A}_1, \dots, \mathbf{A}_n) \in \mathbb{R}^{nm \times nm}$: block diagonal matrix with matrix entries $\mathbf{A}_i \in \mathbb{R}^{m \times m}$, $i \in \{1, \dots, n\}$. $\chi_{\mathbf{A}}(s) := \det[s \mathbf{I}_n - \mathbf{A}]$, characteristic polynomial of $\mathbf{A} \in \mathbb{R}^{n \times n}$. $\arctan2(x, y)$ 2-argument arctangent, for $x, y \in \mathbb{R}$, defined as

$$\arctan2: \mathbb{R}^2 \setminus \{(0, 0)\} \rightarrow (-\pi, \pi], \quad (x, y) \mapsto \arctan2(x, y) := \begin{cases} \arctan\left(\frac{y}{x}\right) & , x > 0 \wedge y \in \mathbb{R} \\ \arctan\left(\frac{y}{x}\right) + \pi & , x < 0 \wedge y > 0 \\ \pm\pi & , x < 0 \wedge y = 0 \\ \arctan\left(\frac{y}{x}\right) - \pi & , x < 0 \wedge y < 0 \\ +\frac{\pi}{2} & , x = 0 \wedge y > 0 \\ -\frac{\pi}{2} & , x = 0 \wedge y < 0. \end{cases} \quad (1)$$

I. INTRODUCTION

A. Motivation and literature review

In view of the increasing number of decentralized generation units with power electronics based grid connection and the decreasing number of large-scale generators, the overall inertia in the grid is diminishing. This results in a faster transient response and higher harmonic distortion of physical quantities (such as currents or voltages) of the power system [2]. Fast frequency fluctuations endanger stability of the power grid. Significant harmonic distortions of voltages and currents can deteriorate power quality and lead to damage or even destruction of grid components. To be capable of taking appropriate countermeasures such as (i) improving stability and quality and (ii) compensating for such deteriorated operation conditions, it is crucial to detect and estimate fundamental and higher harmonic components of the considered quantities in real time as fast and accurate as possible. Hence, grid state estimation became of particular interest to the research community in the last years and has been studied extensively (see e.g. [3], [4], [5], [6], [7], [8], [9], [10], [11], [12], [13], [14], [15], [16], [17], [18], [19], [20], [21], [22], [23], [24], [25] to name a few).

It is well known that a signal with significant harmonic distortion can be decomposed and analyzed by the Fast Fourier Transformation (FFT). However, this method requires a rather long computational time and a large amount of data to be processed [26, p. 320]. Usually, several multiples of the fundamental period (≥ 200 ms) are needed to estimate the harmonics with acceptable accuracy [8]; when the frequency is estimated online as well, the estimation time is even longer.

The majority of the publications deals only with the estimation of fundamental signal parameters (such as amplitude and phase) and fundamental frequency. For signals with negligible harmonic distortion, several well known and rather fast methods

are available [27, Chapter 4] such as *Second-Order Generalized Integrator (SOGI)* or *Adaptive Notch Filters (ANF)* with and without *Phase-Locked Loop (PLL)* [22] or *Frequency Locked-Loop (FLL)* [3], [7]. However, if the signals to be estimated have significant harmonic distortion, these approaches fail and have to be extended by the parallelization of several SOGIs (see e.g. [7], [8], [9], [14], [25]) or several ANFs (see e.g. [4], [5]); each of those being capable of estimating the individual harmonics separately. However, the resulting estimation system is highly nonlinear (in particular in combination with FLL or PLL) and difficult to tune. The estimation speed is usually faster than those of FFT approaches but still rather slow. Other estimation approaches use Adaptive Linear Kalman Filters [28], SOGIs in combination with discrete Fourier transforms [29] or circular limit cycle oscillators [30]. A comparison of estimation speed and estimation accuracy mainly focuses on fundamental signal and frequency estimation. A comparison of all the results presented in the contributions above yields that the estimation speeds vary between 40 – 1 200 ms. The estimation speed depends on the tuning of the estimation algorithms and the operation conditions (such as changing harmonics with varying amplitudes, phases and frequencies) during the estimation process. In particular, when the frequency is changing abruptly, the overall estimation process is drastically decelerated. The FLL can be considered as the bottleneck of grid state estimation. Moreover, the performance of the parallelized estimation of the individual harmonics is mostly not discussed and evaluated.

Exceptions are the contributions [7], [8] and [4]; which explicitly discuss and show the estimation performance of the parallelized SOGIs and ANFs, respectively, for *each* considered harmonic component. For example, in [7], the proposed parallelized SOGIs with FLL (called MSOGI-FLL) are capable of extracting fundamental frequency and amplitudes and phases of a pre-specified number n of harmonics $\nu \in \{\nu_1, \dots, \nu_n\}$. Local stability analysis and tuning of the parallelized SOGIs and FLL were thoroughly discussed. As outcomes of the tuning rules, the gain k_ν of the ν -th SOGI should be chosen to be $k_\nu = \frac{1}{\nu}\sqrt{2} < \frac{1}{\nu}2$ which represents a “tradeoff between settle time, overshooting and harmonic rejection”. Simulation and measurement results were presented for three-phase signals. Six harmonics (including fundamental positive sequence) and the fundamental frequency were correctly estimated. The estimation speeds for the individual harmonics vary between 40 – 140 ms. Frequency estimation takes about 300 ms to return to a constant value. In [8], a similar idea is proposed. The proposed algorithm is also based on parallelized SOGIs but a FLL has not been implemented. If the frequency is known, the method is capable of estimating the harmonics in approximately 40 – 60 ms¹. Only simulation results were presented for seven harmonics. No results were presented when the frequency is unknown and varying. Implementation and tuning of the parallelized SOGIs are hardly discussed. In [4], parallelized ANFs with FLL are implemented. For a constant (estimated) frequency, a complete stability proof for the parallelized structure is presented showing that stability is preserved if all gains are chosen positive. The parallelized ANFs with FLL are implemented in Matlab/Simulink to estimate a signal with six harmonic components (including fundamental). The fundamental frequency of the considered signal undergoes step-like changes of +4 Hz and –2 Hz. Frequency and harmonics estimation errors tend to zero; but the estimation speed is rather slow and varies between 1 – 1,5 s.

As already noted, the (parallelized) SOGIs and ANFs rely on a precise estimate of the fundamental (angular) frequency for proper functionality. If the frequency is known a priori, it can be fed directly to the parallelized systems. Otherwise, the observers must be combined with a FLL (or PLL), which allows to additionally estimate the fundamental angular frequency online. Since the FLL estimation depends on the harmonic amplitudes of the input signal, [7], [17], [15] describe a *Gain Normalization (GN)* which robustifies the frequency estimation. Nevertheless, due to its nonlinear and time-varying dynamics, the tuning of the overall estimator consisting of parallelized SOGIs or ANFs and FLL is a non-trivial task. As a rule of thumb (coming from the steady-state derivation of the FLL adaption law), the tuning of the FLL should be slow compared to the dynamics of the parallelized SOGIs or ANFs and, therefore, significantly degrades the settling time of the overall estimation system [10]. Apart from that, negative estimates of the angular frequency lead to instability. In this context, [12] describes a saturation of the estimated angular frequency to avoid a sign change. However, this saturation does not necessarily (i) ensure convergence of the estimation error or (ii) accelerate the transient response of the FLL. In [24], the FLL is extended by output saturation and anti-windup to avoid too large estimation values. But the proposed anti-windup strategy comes with additional feedback gain (tuning parameter), which, if not properly chosen, might lead to instability. Other approaches for frequency detection are based on *Phase Locked Loops (PLLs)* [19], [11], [13], [21], [22] which can be combined with SOGIs as well. PLL approaches are not considered in this paper.

The remainder of this paper focuses on modifications of the parallelized “standard SOGIs” and the “standard FLL” as introduced in [3] and [7] which will allow to improve estimation speed and estimation accuracy significantly. Key observation which motivates the modifications is that almost all papers above, except [14], do only consider one single tuning factor (gain) for individual SOGI design. This single tuning factor limits the possible estimation performance. In [14], two gains are considered but their influence on the speed of harmonics estimation is not exploited and investigated. Therefore, this work proposes a *modified* (generalized) algorithm which achieves a prescribed settling time of the estimation process. It is capable of estimating amplitudes, angles and angular frequencies of all harmonic components of interest in real time. The proposed

¹Note that, the authors state that the estimation takes less than 20 ms, which seems not correct as can be observed in Fig. 6 and Fig. 8 in [8].

algorithm consists of parallelized *modified* SOGIs tuned by pole placement. The modified SOGIs come with *additional* feedback gains (additional tuning parameters) which provide the required degrees of freedom to ensure a desired (prescribed) settling time. Since the standard FLL was derived and is working for the standard SOGI only (as shown in [7] or [9]), also a *modified* FLL is proposed to guarantee functionality in combination with the parallelized modified SOGIs. The novelty of this paper is characterized by the following five main contributions:

- (i) *Modification (generalization)* of standard SOGIs (sSOGIs) to *modified SOGIs (mSOGIs)* with *prescribed settling time* (see Sections II-B and II-C);
- (ii) *Parallelization* of the mSOGIs and their *tuning by pole placement* (see Section II-D);
- (iii) *Modification (generalization)* of the standard FLL to the *modified FLL (mFLL)* with phase-correct adaption law, sign-correct anti-windup strategy and rate limitation for enhanced functionality in combination with the proposed mSOGIs (see Section III-B);
- (iv) *Theoretical derivation* of the pole placement algorithm and the generalized adaption law for the mFLL (see Appendix E and F, respectively);
- (v) *Implementation and validation* of the proposed estimation algorithm by simulation and measurement results and *Comparison* of the estimation performances of parallelized mSOGIs, sSOGIs and (ANFs) *with* and *without* FLL (see Section IV).

B. Problem statement

Single-phase grid signals (e.g. voltages or currents) with significant and arbitrary harmonic distortion are considered. The considered signals are assumed to have the following form

$$\forall t \geq 0: \quad y(t) := \sum_{\nu \in \mathbb{H}_n} \underbrace{a_\nu(t) \cos(\phi_\nu(t))}_{=: y_\nu(t)} \quad \text{where} \quad \mathbb{H}_n := \{1, \nu_2, \dots, \nu_n\} \subset \mathbb{Q}_{>0}, \quad (2)$$

with fundamental amplitude a_1 , harmonic amplitudes $a_{\nu_2}, \dots, a_{\nu_n} \geq 0$ and angles ϕ_ν (in rad), respectively; where $\nu \in \mathbb{H}_n$ indicates the ν -th harmonic component (per definition $\nu_1 := 1$). Observe that ν does not necessarily need to be a natural number or larger than one; any rational number is admissible as well (e.g. $\nu_2 = 5/3$ or $\nu_3 = 1/5$). Moreover, to consider the most general case, the phase angles

$$\forall \nu \in \mathbb{H}_n \quad \forall t \geq 0: \quad \phi_\nu(t) = \int_0^t \nu \omega(\tau) \, d\tau + \phi_{\nu,0},$$

of the ν -th harmonic component depend on the time-varying angular *fundamental* frequency $\omega(\cdot) := \omega_1(\cdot) > 0 \frac{\text{rad}}{\text{s}}$ and the initial harmonic angle $\phi_{\nu,0} \in \mathbb{R}$. The main goal of this paper is threefold:

- (i) to propose a *modified Second-Order Generalized Integrator (mSOGI)* with *prescribed settling time* for a *fast online estimation* of amplitudes \hat{a}_ν and angles $\hat{\phi}_\nu$, such that, after a *specified* transient phase, estimated signal \hat{y} (indicated by “ $\hat{\cdot}$ ”) and original signal y do not differ more than a given threshold $\varepsilon_y > 0$. More precisely, the following should hold

$$\forall t \geq t_{\text{set}}: \quad |y(t) - \hat{y}(t)| \leq \varepsilon_y \quad \text{where} \quad \hat{y}(t) := \sum_{\nu \in \mathbb{H}_n} \underbrace{\hat{a}_\nu(t) \cos(\hat{\phi}_\nu(t))}_{=: \hat{y}_\nu(t)} \quad (3)$$

after a *prescribed (specified) settling time* $t_{\text{set}} > 0$ s;

- (ii) to propose a *modified Frequency Locked Loop (mFLL)* ensuring stable operation and fast estimation of the angular frequency in combination with the proposed parallelized mSOGIs; and
- (iii) to show the overall estimation performance and compare it to other standard approaches such as parallelized sSOGIs and ANFs with and without FLL.

Remark I.1. Note that in (2), *time-varying amplitudes (of each harmonic component)* and *time-varying angles* are considered. The typical assumption (see, e.g. [27, Appendix A]) of a constant *fundamental angular frequency* $\omega > 0$ such that $\phi_\nu(t) = \nu\omega t$ is not imposed, since it is not true in general.

C. Principle idea of proposed solution

The principle idea of the proposed solution is illustrated in Fig. 1. The depicted block diagram is fed by the input signal y to be estimated. All subsystems of the overall nonlinear observer are shown. The outputs of the block diagram are the respective estimated components of the input signal (see Sect. I-B). In Fig. 1, all components (subsystems) of the nonlinear observer are explicitly shown. One can summarize: For $\nu \in \mathbb{H}_n$, the overall nonlinear observer consists of the following subsystems:

- a *parallelization* of *modified Second-Order Generalized Integrators (mSOGIs)* to estimate amplitude and phase of each of the harmonic components of the input signal y . The ν -th mSOGI will output the estimated state vector

$$\hat{\mathbf{x}}_\nu := (\hat{x}_\nu^\alpha, \hat{x}_\nu^\beta)^\top = (\hat{y}_\nu, \hat{q}_\nu)^\top$$

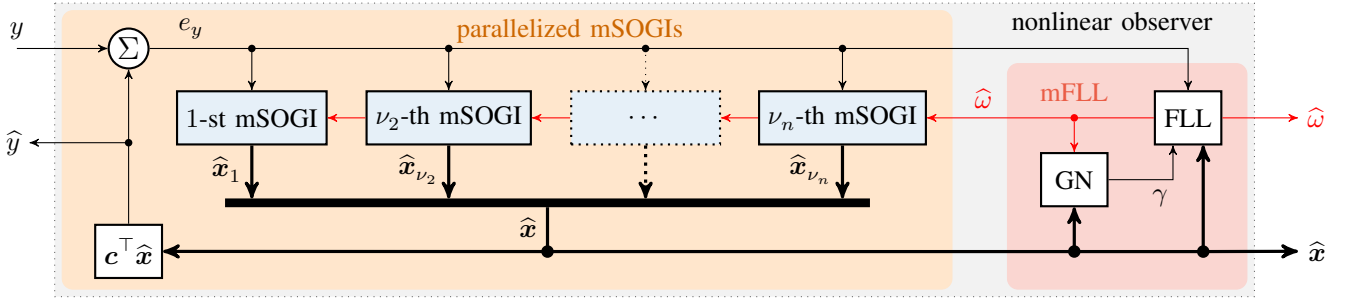


Figure 1: Block diagram of the nonlinear observer (consisting of parallelized mSOGIs and modified FLL (mFLL) with gain normalization (GN)).

compromising estimates of in-phase and quadrature signals of the ν -th harmonic component, i.e. $\hat{y}_\nu = \hat{x}_\nu^\alpha$ and $\hat{q}_\nu = \hat{x}_\nu^\beta$, respectively. All n estimated signal vectors \hat{x}_ν are merged into the overall estimation vector

$$\hat{\mathbf{x}} := \left(\underbrace{(\hat{y}_1, \hat{q}_1)}_{=: \hat{\mathbf{x}}_1^\top}, \underbrace{(\hat{y}_{\nu_2}, \hat{q}_{\nu_2})}_{=: \hat{\mathbf{x}}_{\nu_2}^\top}, \dots, \underbrace{(\hat{y}_{\nu_n}, \hat{q}_{\nu_n})}_{=: \hat{\mathbf{x}}_{\nu_n}^\top} \right)^\top \in \mathbb{R}^{2n}. \quad (4)$$

The output signal $\hat{y} = \sum_{\nu \in \mathbb{H}_n} \hat{y}_\nu = \mathbf{c}^\top \hat{\mathbf{x}}$ represents the estimate of the input signal y and is established by the sum of all estimates of the in-phase signals $\hat{y}_\nu = \hat{x}_\nu^\alpha$ of the mSOGIs;

- a *modified Frequency Locked Loop (mFLL)* with gain normalization, generalized frequency adaption law, sign-correct anti-windup strategy and rate limitation to obtain the estimate $\hat{\omega}$ of the fundamental angular frequency ω . The mFLL is tuned by an adaptive gain γ which depends on estimation input error $e_y := y - \hat{y}$, estimation vector $\hat{\mathbf{x}}$ and estimated angular frequency $\hat{\omega}$;

Section II and Section III introduce the different subsystems (i.e. mSOGIs and mFLL) illustrated in Fig. 1 and explain in more detail their contribution to the proposed solution for real-time estimation of amplitudes and phases of all n harmonics of the input signal y as in (2) as well as the fundamental frequency ω .

II. SECOND-ORDER GENERALIZED INTEGRATORS (SOGIs): IN-PHASE AND QUADRATURE SIGNAL ESTIMATION

The key tool to estimate in-phase and quadrature signals of a measured sinusoidal signal is a *Second-Order Generalized Integrator (SOGI)* [27, App. A]. Their parallelization in combination with a FLL (see Sect. III) allows to detect all harmonic components and the fundamental frequency. First, a standard SOGI (as e.g. discussed in [7]) for the ν -th harmonic is revisited. After that, the proposed modification to it is introduced to obtain the modified SOGI with prescribed settling time. It is shown that the modified SOGI is actually a generalization of the standard SOGI. Next, their estimation performances are compared. Finally, to be capable of estimating all n harmonics, the proposed modified (or standard) SOGIs are parallelized to obtain the overall observer system. Throughout this paper, the more powerful state space representation will be used, since the considered parallelized SOGIs with FLL represent a nonlinear system and transfer functions are not applicable.

A. Standard SOGI (sSOGI) for the ν -th harmonic component [7]

For now, let $\nu \in \mathbb{H}_n$ and consider only the ν -th harmonic component $y_\nu(t) := a_\nu(t) \cos(\phi_\nu(t))$. If the estimate $\hat{\omega}_\nu := \nu \hat{\omega}$ of the ν -th harmonic frequency is known, the implementation of a sSOGI for the signal y_ν allows to obtain *online* estimates $\hat{y}_\nu = \hat{x}_\nu^\alpha$ and $\hat{q}_\nu = \hat{x}_\nu^\beta$ of in-phase and quadrature signal, respectively. A sSOGI for the ν -th harmonic component is depicted in Fig. 2(a). Its dynamics are given by the following time-varying differential equation

$$\left. \begin{aligned} \frac{d}{dt} \underbrace{\begin{pmatrix} \hat{x}_\nu^\alpha(t) \\ \hat{x}_\nu^\beta(t) \end{pmatrix}}_{=: \hat{\mathbf{x}}_\nu(t) \in \mathbb{R}^2} &= \hat{\omega}(t) \underbrace{\begin{bmatrix} -\nu k_\nu & -\nu \\ \nu & 0 \end{bmatrix}}_{=: \mathbf{A}_\nu(k_\nu) \in \mathbb{R}^{2 \times 2}} \hat{\mathbf{x}}_\nu(t) + \hat{\omega}(t) \underbrace{\begin{pmatrix} \nu k_\nu \\ 0 \end{pmatrix}}_{=: \mathbf{l}_\nu(k_\nu) \in \mathbb{R}^2} y_\nu(t), & \hat{\mathbf{x}}_\nu(0) = \hat{\mathbf{x}}_{\nu,0} \in \mathbb{R}^2 \\ \hat{y}_\nu(t) &= \underbrace{\begin{pmatrix} 1, & 0 \end{pmatrix}}_{=: \mathbf{c}_\nu^\top \in \mathbb{R}^{1 \times 2}} \hat{\mathbf{x}}_\nu(t) \end{aligned} \right\} \quad (5)$$

with arbitrary initial value $\hat{\mathbf{x}}_{\nu,0} \in \mathbb{R}^2$ (mostly set to zero), gain $k_\nu > 0$ (*single tuning factor*) and estimate $\hat{\omega}$ (possibly time-varying) of the fundamental angular frequency ω . The gain k_ν only allows for a *limited* tuning of the dynamic response of the sSOGI. For constant $\hat{\omega} > 0$ only, characteristic equation and poles of the ν -th sSOGI are given as follows²

$$\chi_\nu(s) := \det[s\mathbf{I}_2 - \hat{\omega}\mathbf{A}_\nu] = s^2 + \nu\hat{\omega}k_\nu s + (\nu\hat{\omega})^2 \stackrel{!}{=} 0 \implies p_{\nu,1/2} = -\frac{\nu\hat{\omega}k_\nu}{2} \left(1 \pm \sqrt{1 - \frac{4}{k_\nu^2}} \right). \quad (6)$$

²Note that for time-varying or nonlinear systems, the analysis of poles is *not* sufficient to check stability [31, Example 3.3.7].

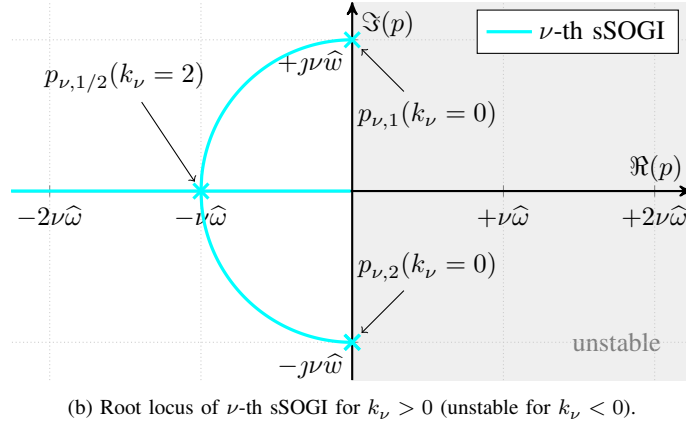
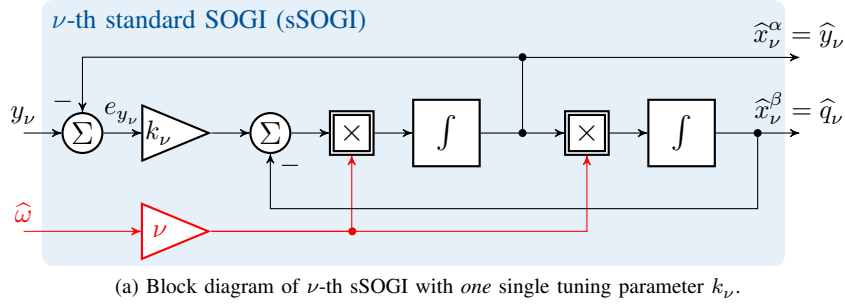


Figure 2: Standard Second-Order Generalized Integrator (sSOGI) [7]: (a) Block diagram and (b) root locus of ν -th sSOGI.

The respective root locus is shown in Fig. 2 (b). Hence, stability is guaranteed for all $k_\nu > 0$. However, since the pole closest to the imaginary axis determines the settling time of the system, the smallest settling time is obtained for $k_\nu = 2$ which clearly limits the tuning of the transient performance of the sSOGI. Moreover, this choice leads to two real poles at $-\frac{\nu\hat{\omega}k_\nu}{2}$ and, hence, the sSOGI is *not* capable of oscillating by itself. Therefore, common tunings are $k_\nu = \sqrt{2}/\nu$ [7] or $k_\nu = 1$ [4].

B. Modified SOGI (mSOGI) for the ν -th harmonic component

To overcome the problem of the limited tuning without the possibility to prescribe the settling time, the modified SOGI (mSOGI) with additional gain g_ν is introduced. The resulting block diagram of the ν -th mSOGI is illustrated in Fig. 3 (a). Note that the additional gain does *not* impair functionality but gives the necessary degree of freedom to enhance the transient performance as will be shown in the next subsection. The state space representation of the ν -th mSOGI is given by the following time-varying differential equation:

$$\left. \begin{aligned} \frac{d}{dt} \hat{\mathbf{x}}_\nu(t) &= \hat{\omega}(t) \underbrace{\begin{bmatrix} -\nu k_\nu & -\nu \\ \nu(1-g_\nu) & 0 \end{bmatrix}}_{=: \mathbf{A}_\nu(k_\nu, g_\nu)} \hat{\mathbf{x}}_\nu(t) + \hat{\omega}(t) \underbrace{\begin{pmatrix} \nu k_\nu \\ \nu g_\nu \end{pmatrix}}_{=: \mathbf{l}_\nu(k_\nu, g_\nu)} y_\nu(t), & \hat{\mathbf{x}}_\nu(0) &= \hat{\mathbf{x}}_{\nu,0} \in \mathbb{R}^2 \\ \hat{y}_\nu(t) &= \mathbf{c}_\nu^\top \hat{\mathbf{x}}_\nu(t) \end{aligned} \right\} \quad (7)$$

with arbitrary initial value $\hat{\mathbf{x}}_{\nu,0} \in \mathbb{R}^2$ and estimate $\hat{\omega}$ of ω . The gains k_ν and g_ν now allow (theoretically³) for a *limitless* tuning of the dynamic response of the mSOGI. The tiny but crucial difference between the mSOGI in (7) and the sSOGI in (5) is the additional gain g_ν in the system matrix $\mathbf{A}_\nu(k_\nu, g_\nu)$ and the vector $\mathbf{l}_\nu(k_\nu, g_\nu)$. For a constant frequency $\hat{\omega}$, the characteristic equation and the poles of the ν -th mSOGI are given by

$$\begin{aligned} \chi_\nu(s) := \det[s\mathbf{I}_2 - \hat{\omega}\mathbf{A}_\nu] &= s^2 + \nu\hat{\omega}k_\nu s + (1-g_\nu)(\nu\hat{\omega})^2 \stackrel{!}{=} 0 & \implies & p_{\nu,1/2} = -\frac{\nu\hat{\omega}k_\nu}{2} \left(1 \pm \sqrt{1 - 4\frac{(1-g_\nu)}{k_\nu^2}} \right) \\ & & \implies & g_\nu = -\frac{k_\nu^2}{4} \\ & & \implies & p_{\nu,1/2} = -\frac{\nu\hat{\omega}k_\nu}{2} \pm j\nu\hat{\omega}. \end{aligned} \quad (8)$$

³Of course, noise will limit the feasible tuning.

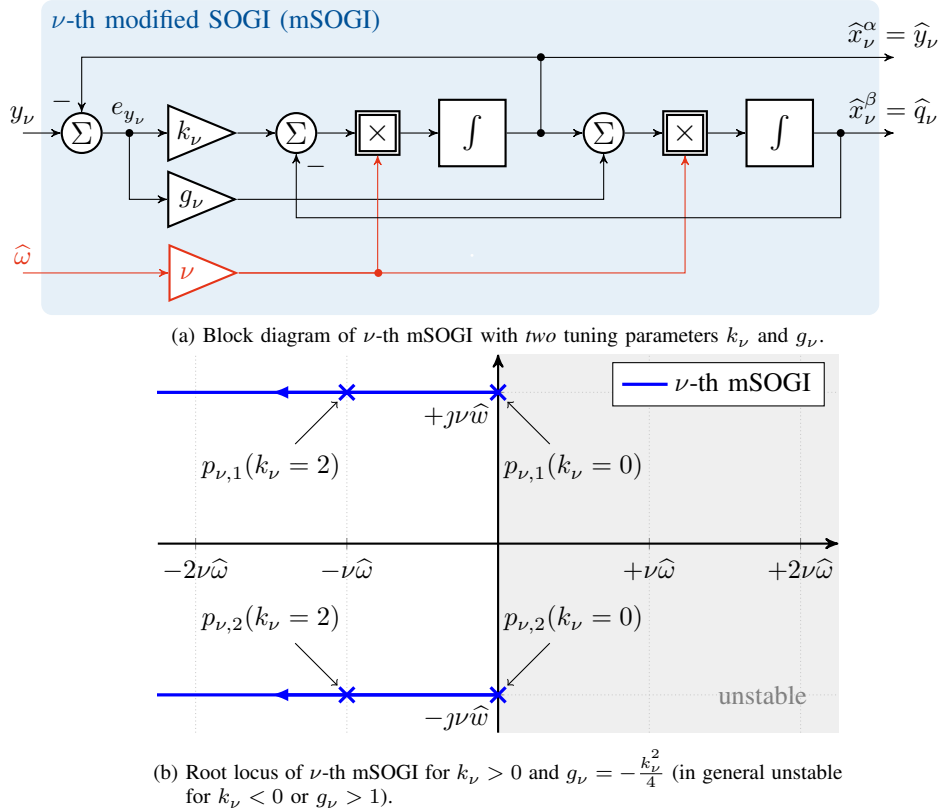


Figure 3: Modified Second-Order Generalized Integrator (mSOGI): (a) Block diagram and (b) root locus of ν -th mSOGI.

The special choice of the additional gain $g_\nu = -\frac{k_\nu^2}{4}$ in (8) gives the key feature of the mSOGI: For any $k_\nu > 0$, the real parts of the poles $p_{\nu,1/2}$ in (8) can be chosen arbitrarily; whereas the capability of the mSOGI to oscillate with angular frequency $\nu\hat{\omega}$ is preserved (see imaginary parts of $p_{\nu,1/2}$). The root locus of the ν -th mSOGI is depicted in Fig. 3(b). The mSOGI is stable for any $k_\nu > 0$; and, the larger k_ν is chosen, the faster is its transient response.

Remark II.1 (Generalization of the sSOGI). *The introduction of the additional gain g_ν for the mSOGI in (7) represents actually a generalization of the sSOGI in (5). Clearly, for $g_\nu = 0$, the mSOGI simplifies to the sSOGI. In other words, only now, the term “second-order generalized integrator” is really appropriate.*

C. Comparison of the estimation performances of sSOGI and mSOGI

If $\hat{\omega} = \omega$, both SOGIs are capable of estimating in-phase signal $\hat{y}_\nu = \hat{x}_\nu^\alpha$ and quadrature signal $\hat{q}_\nu = \hat{x}_\nu^\beta$ of the ν -th harmonic signal $y_\nu(t) := a_\nu(t) \cos(\phi_\nu(t))$. The estimated amplitude

$$\hat{a}_\nu(t) := \|\hat{\mathbf{x}}_\nu(t)\| = \sqrt{\hat{y}_\nu(t)^2 + \hat{q}_\nu(t)^2} \quad (9)$$

is given by the norm of the estimated signal and its quadrature signal. The estimated phase angle is given by

$$\hat{\phi}_\nu(t) = \arctan2(\hat{y}_\nu(t), \hat{q}_\nu(t)) \quad \text{with} \quad \arctan2(\cdot, \cdot) \text{ as in (1)}. \quad (10)$$

Hence, the parameters \hat{a}_ν and $\hat{\phi}_\nu$ of the ν -th harmonic can be detected online.

In Fig. 4, the transient responses of sSOGI and mSOGI are shown in cyan and blue, respectively, for the first harmonic (i.e. $\nu = 1$, see Fig. 4(a)) and for second harmonic (i.e. $\nu = 2$, see Fig. 4(b)). Four tunings of the gain k_ν are implemented and illustrated by different line types: $k_\nu = 0.5$ (dotted), $k_\nu = 1$ (dashed), $k_\nu = 2$ (dash-dotted) and $k_\nu = 10$ (solid). The larger k_ν is chosen, the faster is the transient response of the mSOGI. Moreover, for $k_\nu = 2$ (dash-dotted) or $k_\nu = 10$ (solid), settling times of e.g. $t_{\text{set}} = 0,01$ s and $t_{\text{set}} = 0,005$ s can be guaranteed for the fundamental signal, respectively. For the second harmonic, the transient response is twice as fast as for the fundamental signal. For the sSOGI, a prescribed settling time *cannot* be ensured, since one pole approaches the imaginary axis for large choices of k_ν (see also Fig. 2). In particular, the estimation of the quadrature component is slow (see e_q in Fig. 4) which degrades the estimation speed of positive, negative and zero sequences in three-phase systems (not considered in this paper).

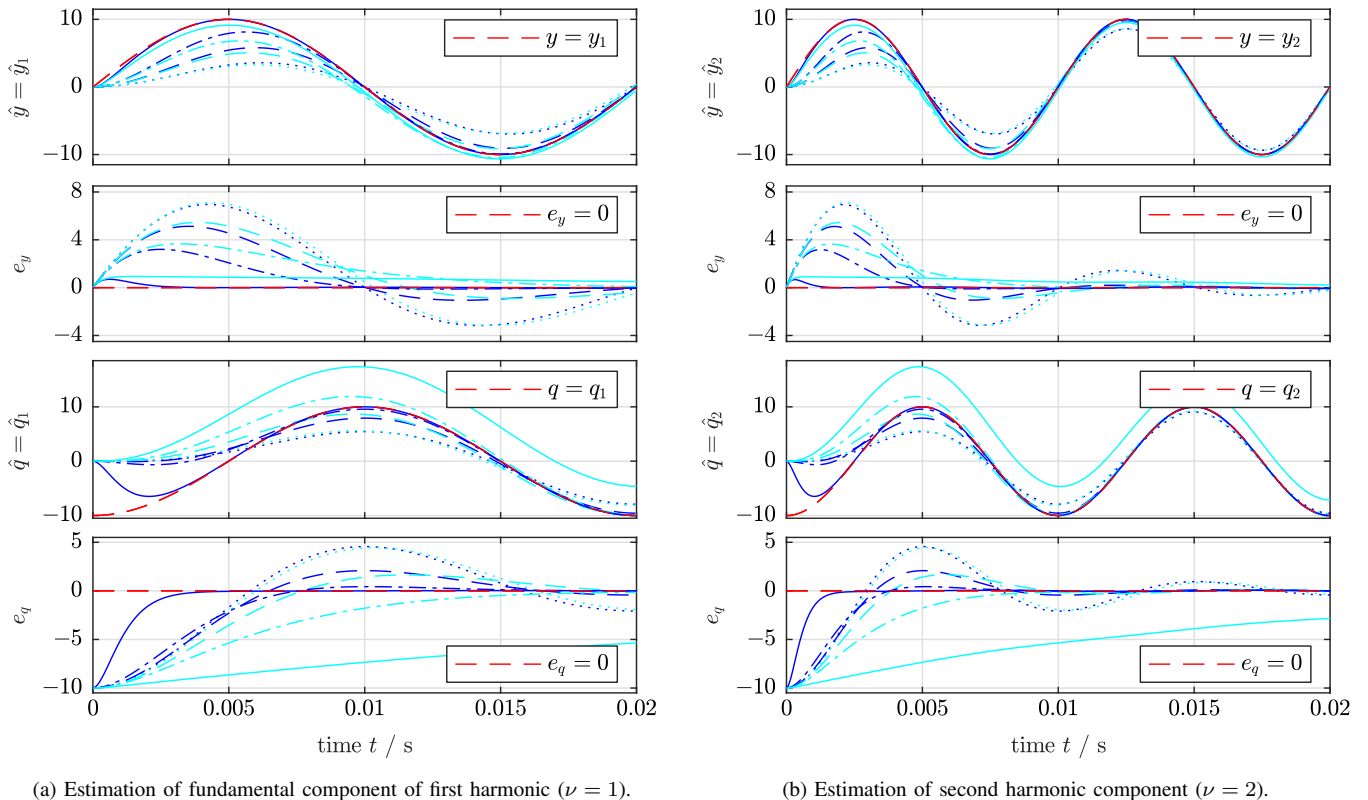


Figure 4: Comparison of estimation performances of ν -th sSOGI (....., - - - - , - - - - , - - - -) and ν -th mSOGI (....., - - - - , - - - - , - - - -) for four different tunings of gain $k_\nu \in \{0.5, 1, 2, 10\}$, respectively. Signals shown in (a) for $\nu = 1$ and in (b) for $\nu = 2$ are from top to bottom: input signal y_ν and its estimate \hat{y}_ν , estimation in-phase error $e_y = y_\nu - \hat{y}_\nu$, quadrature signal q_ν and its estimate \hat{q}_ν and estimation quadrature error $e_q = q_\nu - \hat{q}_\nu$.

D. Parallelization of the mSOGIs

This far, the presented SOGIs (sSOGIs and mSOGIs) can only estimate in-phase signal $\hat{y}_\nu = \hat{x}_\nu^\alpha$ and quadrature signal $\hat{q}_\nu = \hat{x}_\nu^\beta$ of the ν -th harmonic signal $y_\nu(t) := a_\nu(t) \cos(\phi_\nu(t))$. By parallelizing n of the mSOGIs or sSOGIs (see Fig. 1), it is possible to extract in-phase and quadrature signal of each harmonic component y_ν for all $\nu \in \mathbb{H}_n$. For the parallelized sSOGIs, stability is preserved for a positive choice of all gains, i.e. $k_\nu > 0$ for all $\nu \in \mathbb{H}_n$ [4]. Stability for the parallelized mSOGIs will be guaranteed by pole placement. Moreover, the settling time can only be pre-specified by the parallelized mSOGIs.

The idea of the parallelization can be motivated by recalling the *internal model principle* which states that "[e]very good regulator [or observer] must incorporate a model of the outside world being capable to reduplicate the dynamic structure of the exogenous signals which the regulator [or observer] is required to process." [32]. In the considered case, the exogenous signal y as in (2) can be reduplicated by the parallelization of n sinusoidal internal models [33, Chapter 20], which have the overall dynamics

$$\left. \begin{aligned} \frac{d}{dt} \mathbf{x}(t) &= \omega(t) \mathbf{J} \mathbf{x}(t), & \mathbf{x}(0) &= \mathbf{x}_0 \neq \mathbf{0}_{2n} \in \mathbb{R}^{2n} \\ y(t) &= \underbrace{(1, 0, 1, 0, \dots, 1, 0)}_{=: \mathbf{c}^\top \in \mathbb{R}^{2n}} \mathbf{x}(t) \end{aligned} \right\} \quad (11)$$

where

$$\mathbf{x} := \underbrace{\left(\underbrace{(x_1^\alpha, x_1^\beta)}_{=: \mathbf{x}_1^\top}, \dots, \mathbf{x}_n^\top \right)^\top}_{=: \mathbf{x}_1^\top}, \quad \mathbf{J} := \text{blockdiag}(\bar{\mathbf{J}}, \nu_2 \bar{\mathbf{J}}, \dots, \nu_n \bar{\mathbf{J}}) \in \mathbb{R}^{2n \times 2n} \quad \text{and} \quad \bar{\mathbf{J}} = \begin{bmatrix} 0 & -1 \\ 1 & 0 \end{bmatrix} = -\bar{\mathbf{J}}^\top = -\bar{\mathbf{J}}^{-1}. \quad (12)$$

The initial values of the internal model in (11) allow to determine amplitude a_ν and angle ϕ_ν of the ν -th harmonic. For constant $\omega > 0$ and differing harmonics $\nu_i \neq \nu_j$ for all $i \neq j \in \{1, \dots, n\}$, the overall internal model (11) is completely state observable (see Proposition A.1 in the appendix).

Now, by substituting estimate $\hat{\omega}$ for ω , the observer is obtained and consists of the parallelized mSOGIs (as introduced in (7))

for the ν -th harmonic). The observer dynamics are nonlinear and given by

$$\left. \begin{aligned} \frac{d}{dt} \hat{\mathbf{x}}(t) &= \hat{\omega}(t) \mathbf{J} \hat{\mathbf{x}}(t) + \hat{\omega}(t) \mathbf{l} \left(y(t) - \underbrace{\mathbf{c}^\top \hat{\mathbf{x}}(t)}_{=\hat{y}(t)} \right) \\ &= \hat{\omega}(t) \underbrace{[\mathbf{J} - \mathbf{l} \mathbf{c}^\top]}_{=\mathbf{A}} \hat{\mathbf{x}}(t) + \hat{\omega}(t) \mathbf{l} y(t), & \hat{\mathbf{x}}(t) = \hat{\mathbf{x}}_0 \in \mathbb{R}^{2n} \\ \hat{y}(t) &= \underbrace{(\mathbf{c}_1^\top, \mathbf{c}_{\nu_2}^\top, \dots, \mathbf{c}_{\nu_n}^\top)}_{\stackrel{(11), (7)}{=} \mathbf{c}^\top} \hat{\mathbf{x}}(t), \end{aligned} \right\} \quad (13)$$

where observer state vector $\hat{\mathbf{x}} \stackrel{(7)}{=} (\hat{\mathbf{x}}_1^\top, \hat{\mathbf{x}}_{\nu_2}^\top, \dots, \hat{\mathbf{x}}_{\nu_n}^\top)^\top \in \mathbb{R}^{2n}$ and observer gain vector

$$\mathbf{l} := (\mathbf{l}_1^\top, \mathbf{l}_{\nu_2}^\top, \dots, \mathbf{l}_{\nu_n}^\top)^\top \stackrel{(7)}{=} (k_1, g_1, \dots, \nu_n k_n, \nu_n g_n)^\top \in \mathbb{R}^{2n} \quad (14)$$

merge the individual sub-state estimation vectors $\hat{\mathbf{x}}_\nu$ and gain vectors \mathbf{l}_ν of the ν mSOGIs as in (7). The observer will be tuned by pole placement and, hence, the gains in \mathbf{l} can be determined by comparing the coefficients of the characteristic polynomial

$$\chi_{\mathbf{A}}(s) = \prod_{i=1}^n (s^2 + \nu_i^2) - \sum_{i=1}^n g_i \nu_i^2 \prod_{\substack{k=1 \\ k \neq i}}^n (s^2 + \nu_k^2) + s \sum_{i=1}^n k_i \nu_i \prod_{\substack{k=1 \\ k \neq i}}^n (s^2 + \nu_k^2) \quad (15)$$

of the closed-loop system matrix $\mathbf{A} := \mathbf{J} - \mathbf{l} \mathbf{c}^\top$ in (13) and the coefficients of a desired polynomial

$$\chi_{\mathbf{A}^*}(s) := \prod_{i=1}^{2n} (s - p_i^*) \quad (16)$$

with $2n$ prescribed stable roots (poles) $p_i^* \in \mathbb{C}_{<0}$, $i \in \{1, \dots, 2n\}$, in the negative complex half-plane. The detailed derivation of the analytical solution of the pole placement algorithm is presented in Appendix E. The resulting feedback gain vector \mathbf{l} is obtained as follows

$$\mathbf{l} = \mathbf{S} \tilde{\mathbf{p}}_{\mathbf{A}}^*, \quad (17)$$

where

$$\mathbf{S} := \begin{bmatrix} \mathbf{S}_{1,1} & \cdots & \mathbf{S}_{n,1} \\ \vdots & \ddots & \vdots \\ \mathbf{S}_{1,n} & \cdots & \mathbf{S}_{n,n} \end{bmatrix}, \quad \mathbf{S}_{c,r} := (-1)^{c+1} \nu_r^{2(n-c)} \mathbf{R}_r \prod_{\substack{i=1 \\ i \neq r}}^n (\nu_r^2 - \nu_i^2)^{-1} \quad \text{and} \quad \mathbf{R}_i := \begin{bmatrix} 1 & 0 \\ 0 & -\frac{1}{\nu_i} \end{bmatrix} \quad (18)$$

and

$$\tilde{\mathbf{p}}_{\mathbf{A}}^* := \left(-\sum_{i=1}^{2n} p_i^*, \sum_{i=1}^{2n} p_i^* \sum_{j=i+1}^{2n} s_j - \sum_{i=1}^n \nu_i^2, -\sum_{i=1}^{2n} p_i^* \sum_{j=i+1}^{2n} p_j^* \sum_{k=j+1}^{2n} p_k^*, \dots, \prod_{i=1}^{2n} p_i^* - \prod_{i=1}^n \nu_i^2 \right)^\top. \quad (19)$$

It can be shown that, for any positive (but possibly time-varying) angular frequency estimate $\hat{\omega}(t) \geq \varepsilon_\omega > 0$ for all $t \geq 0$, the closed-loop observer system (13) is bounded-input bounded-output (BIBO) stable and input-to-state stable (ISS). Moreover, if $\hat{\omega} \rightarrow \omega$, then the estimation state error $e_x := \mathbf{x} - \hat{\mathbf{x}} \rightarrow \mathbf{0}_{2n}$ decays exponentially to zero (see Theorem A.2, Theorem A.3 and Remark A.4 in the appendix).

Remark II.2 (place command in Matlab versus analytical expression in (17)). *For small n (e.g. $n \leq 10$), the Matlab command `place` can be used to compute $\mathbf{l} = \text{place}(\mathbf{J}', \mathbf{c}, \dots)$. For large n , `place` might not provide a proper result. Moreover, `place` cannot place poles with multiplicity greater than $\text{rank}(\mathbf{c}) = 1$. That is why, the analytical expression in (17) has been derived. It can be used to achieve pole placement for arbitrarily large n .*

III. FREQUENCY-LOCKED LOOP (FLL): FREQUENCY ESTIMATION

As mentioned above, a correct estimate of the fundamental angular frequency is essential for a proper functionality of the parallelized SOGIs and the harmonics detection. The following subsections motivate and discuss the necessary modifications of the FLL to ensure its functionality also with the parallelized mSOGIs.

A. Standard FLL (sFLL) [7]

In this subsection, the standard FLL is re-visited. Its block diagram is shown in Fig. 5. Adaption law and gain normalization are briefly explained.

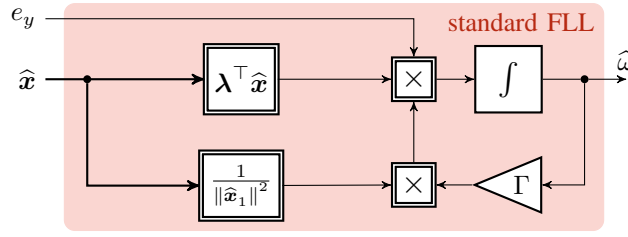


Figure 5: Block diagram of standard Frequency Locked Loop (sFLL) with gain normalization [4], [7], [17].

1) *Adaption law*: As shown in Fig. 1, any of the n parallelized mSOGIs requires an estimate $\hat{\omega}$ of the fundamental angular frequency ω . The estimate $\hat{\omega}$ is the output of the FLL. The nonlinear adaption law of the sFLL is given by [7]

$$\frac{d}{dt}\hat{\omega}(t) = \gamma(t)\lambda^\top \hat{\mathbf{x}}(t)e_y(t) \stackrel{[4]}{=} \gamma(t)k_1\hat{x}_1^\beta(t)e_y(t), \quad \hat{\omega}(0) = \hat{\omega}_0 \in \mathbb{R}, \quad (20)$$

where $\gamma(\cdot) > 0$ is a positive but non-constant adaptive gain, $\lambda = (0, -k_1, \mathbf{0}_{2n-2}^\top)^\top$ [4], [7] is a constant "selection" vector (to extract only the fundamental estimate \hat{x}_1^β from $\hat{\mathbf{x}}$), $\hat{\mathbf{x}}$ is the estimation vector of the parallelized sSOGIs and $e_y := y - \hat{y}$ is the estimation error (difference between input y and estimated input \hat{y}). A proper choice of the initial value, e.g. $\hat{\omega}_0 \in \{2\pi 50, 2\pi 60\}$, of the sFLL adaption law is beneficial for functionality and adaption speed.

Remark III.1 (Impact of negative estimates of the angular frequency). *Note that, in view of the adaption law in (20), the estimated angular frequency might also become negative, i.e. $\hat{\omega}(\tau) < 0$ for some time instant $\tau \geq 0$. However, a negative $\hat{\omega} < 0$ will result in instability of the parallelized sSOGIs and all estimated states will diverge.*

2) *Gain Normalization (GN)*: The FLL should be robustified to work for signals with arbitrary fundamental amplitudes and angular frequencies (see [7], [17]). This can be achieved by introducing the following adaptive sFLL gain

$$\gamma(t) := \Gamma \frac{\hat{\omega}(t)}{\|\hat{\mathbf{x}}_1(t)\|^2} \implies \frac{d}{dt}\hat{\omega} = \Gamma \frac{\hat{\omega}(t)}{\|\hat{\mathbf{x}}_1(t)\|^2} k_1 \hat{x}_1^\beta(t) e_y(t), \quad (21)$$

which depends on gain $\Gamma > 0$, frequency estimate $\hat{\omega}$ and norm of the *fundamental* estimation vector $\hat{\mathbf{x}}_1 = (\hat{x}_1^\alpha, \hat{x}_1^\beta)^\top$ leading to a "normalized" FLL adaption law. The gain $\Gamma > 0$ is a *constant* tuning factor of the FLL.

Remark III.2 (Avoiding division by zero). *Depending on the initial values $\hat{\mathbf{x}}(0)$ and the time evolution of estimation process, the denominator $\|\hat{\mathbf{x}}_1(t)\|^2$ in (21) might become zero for certain time instants $t \geq 0$. This must and can easily be avoided by introducing a minimal positive value for the denominator by substituting $\max(\|\hat{\mathbf{x}}_1(t)\|^2, \varepsilon)$ for $\|\hat{\mathbf{x}}_1(t)\|^2$ in (21) where $\varepsilon > 0$ is a small positive constant.*

B. Modified FLL (mFLL)

The FLL is the weakest subsystem (bottleneck) of the overall grid estimation system; in particular, its tuning endangers system stability, estimation accuracy and estimation speed. Only if the frequency is detected correctly, the mSOGIs or sSOGIs work properly. Therefore, to improve stability and performance of the estimation process a modified FLL is proposed. The block diagram of the proposed mFLL is depicted in Fig. 6. Remarks III.1 and III.2 have already been considered in the block diagram. In addition, the mFLL is equipped with a generalized adaption law, a sign-correct anti-windup strategy and a rate limitation. All three modifications enhance performance and stability of the mFLL. The generalized adaption law increases adaption speed. The anti-windup strategy guarantees that the estimated angular frequency $\hat{\omega}$ remains bounded and positive for all time and the rate limitation prevents too fast adaption speeds which might endanger stability. Details will be explained in the next subsections.

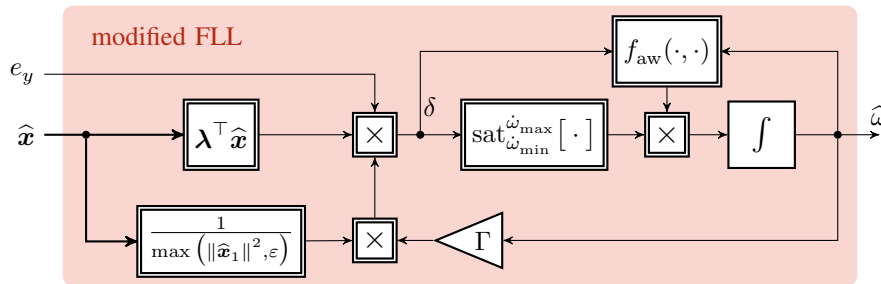


Figure 6: Modified Frequency Locked Loop (mFLL) with gain normalization, sign-correct anti-windup and rate limitation.

1) *Generalized adaption law*: The presented adaption law (20) of the sFLL does not work properly for the mSOGIs. It does *not* guarantee a sign-correct adaption for all time. Therefore, the adaption law must be generalized to fit to the parallelized mSOGIs. It is clear that for a sign-correct adaption of the estimated angular frequency $\hat{\omega}$, the generalized adaption law must ensure that the following conditions hold

$$\left. \begin{aligned} \forall \hat{\omega} < \omega \wedge e_y \neq 0 &\implies \frac{d}{dt}\hat{\omega} \propto \boldsymbol{\lambda}^\top \hat{\boldsymbol{x}} e_y > 0, \\ \forall \hat{\omega} = \omega \wedge e_y \neq 0 &\implies \frac{d}{dt}\hat{\omega} \propto \boldsymbol{\lambda}^\top \hat{\boldsymbol{x}} e_y = 0 \quad \text{and} \\ \forall \hat{\omega} > \omega \wedge e_y \neq 0 &\implies \frac{d}{dt}\hat{\omega} \propto \boldsymbol{\lambda}^\top \hat{\boldsymbol{x}} e_y < 0. \end{aligned} \right\} \quad (22)$$

To illustrate the intuition behind these conditions, assume that the input signal has a constant fundamental angular frequency $\omega > 0$ and that the parallelized mSOGIs are fed by an arbitrary positive but constant estimate $0 < \hat{\omega} \neq \omega$. Then, in *steady state*, the system states $\hat{\boldsymbol{x}}(t)$ with their characteristic amplitude and phase responses can be used to analyze whether e_y and $\boldsymbol{\lambda}^\top \hat{\boldsymbol{x}}$ are *in-phase* or *counter-phase*. In Appendix F3, it is shown that this sign-correct adaption is guaranteed when the selection vector $\boldsymbol{\lambda}$ is chosen as follows

$$\boldsymbol{\lambda} := \text{blockdiag} \left(\boldsymbol{J}^{-1}, \boldsymbol{O}_{2 \times 2}, \dots, \boldsymbol{O}_{2 \times 2} \right) \boldsymbol{l} = (g_1, -k_1, \boldsymbol{0}_{2n-2}^\top)^\top \in \mathbb{R}^{2n}. \quad (23)$$

This choice of $\boldsymbol{\lambda}$ can be used for sSOGI *and* mSOGI as well. It is actually a generalization of the standard choice $\boldsymbol{\lambda} = (0, -k_1, \boldsymbol{0}_{2n-2}^\top)^\top = \text{blockdiag} \left(\boldsymbol{J}^{-1}, \boldsymbol{O}_{2 \times 2}, \dots, \boldsymbol{O}_{2 \times 2} \right) \boldsymbol{l}$ with $g_\nu = 0$ for all $\nu \in \mathbb{H}_n$ (recall (20)). Finally, note that the sign-correct adaption was derived based on a steady state analysis (see Appendix F3). This implies that the mFLL (and sFLL) dynamics should be slow compared to the dynamics of the parallelized mSOGIs (which can be achieved by an adequate choice of Γ).

2) *Sign-correct anti-windup strategy*: Usually, the grid frequency should not exceed a certain interval. This physically motivated limitation can be exploited for the frequency estimation. The principle idea of the proposed sign-correct anti-windup strategy is illustrated in Fig. 7. More precisely, the adaption of the estimated angular frequency shall be stopped (i.e. $\frac{d}{dt}\hat{\omega} = 0$), when

- the estimated angular frequency $\hat{\omega}$ leaves the admissible interval, i.e. $\hat{\omega} \notin (\omega_{\min}, \omega_{\max})$ with lower and upper limit $0 < \omega_{\min} < \omega_{\max}$, respectively (see Fig. 7); and
- the right hand side of the adaption law (22) has wrong sign (otherwise the estimation gets stuck at one of the limits).

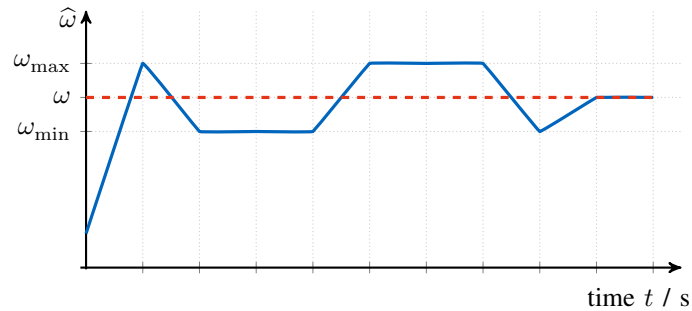


Figure 7: Illustration of the principle idea of the proposed sign-correct anti-windup strategy.

This yields to the following sign-correct anti-windup decision function

$$f_{\text{aw}}(\hat{\omega}, \delta) := \begin{cases} 0, & \text{for } (\hat{\omega} \geq \omega_{\max} \wedge \delta \propto \frac{d}{dt}\hat{\omega} \geq 0) \vee (\hat{\omega} \leq \omega_{\min} \wedge \delta \propto \frac{d}{dt}\hat{\omega} \leq 0) \\ 1, & \text{else} \end{cases} \quad (24)$$

where $\delta \propto \frac{d}{dt}\hat{\omega}$ is proportional to the time derivative of the estimated angular frequency as can be seen when decision function and frequency adaption law are combined as follows

$$\frac{d}{dt}\hat{\omega} = f_{\text{aw}}(\hat{\omega}, \delta) \underbrace{\frac{\Gamma \hat{\omega} e_y \boldsymbol{\lambda}^\top \hat{\boldsymbol{x}}}{\max(\|\hat{\boldsymbol{x}}_1\|^2, \varepsilon)}}_{=: \delta}. \quad (25)$$

The consequences of this adaption law with sign-correct anti-windup are that the estimated angular frequency is *positive* and remains *bounded* for all time, i.e. $\hat{\omega}(t) \in [\min(\hat{\omega}_0, \omega_{\min}), \max(\hat{\omega}_0, \omega_{\max})]$ for all $t \geq 0$. Moreover, once within the admissible interval $[\omega_{\min}, \omega_{\max}]$, the estimated angular frequency will remain inside this interval. Clearly, if the initial value $\hat{\omega}_0$ of the frequency estimate starts outside of $[\omega_{\min}, \omega_{\max}]$, it will approach the interval due to the sign-correct frequency adaption (as illustrated in Fig. 7 for $\hat{\omega}_0 < \omega_{\min}$). Note that the proposed anti-windup strategy does not require tuning of an additional

feedback gain as in [24]. Instability can *not* occur, since the proposed sign-correct anti-windup strategy is based on the simple idea of *conditional integration* [33, Section 10.4.1].

3) *Rate limitation*: Recall that the overall observer (7) is nonlinear. Considering the estimated angular frequency as time-varying parameter, the observer becomes a time-varying linear system. If the time derivative $\frac{d}{dt}\hat{\omega}$ is limited (*rate limitation*), the observer can be considered as *slowly* time-varying system [34] (which simplifies stability analysis). For this *rate limitation* of the adaption law, the admissible rate of the estimated angular frequency must be bounded, i.e. $\frac{d}{dt}\hat{\omega} \in [\dot{\omega}_{\min}, \dot{\omega}_{\max}]$ where $\dot{\omega}_{\min} < 0$ and $\dot{\omega}_{\max} > 0$ are desired lower and upper thresholds, respectively. The idea of the rate limitation is illustrated in the graph shown in Fig. 8.

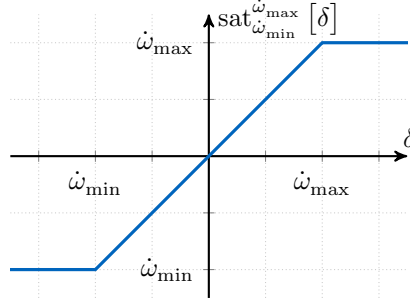


Figure 8: Illustration of the rate limitation of $\delta \propto \frac{d}{dt}\hat{\omega}$.

Usually, the rate limitation leads to a smoother adaption and $\dot{\omega}_{\min} = -\dot{\omega}_{\max}$ is a meaningful choice. Reasonable rate thresholds were found out to be 10 – 100 Hz per 1 ms. The rate limitation can be ensured by introducing an additional saturation function to the adaption law (25) leading to the generalized adaption law for the mFLL as shown next.

C. Generalized adaption law

Finally, combining rate limitation, sign-correct anti-windup strategy and sFLL with gain normalization, the generalized adaption law of the mFLL with λ as in (23) can be introduced. It is given by

$$\frac{d}{dt}\hat{\omega} = f_{aw}(\hat{\omega}, \delta) \cdot \text{sat}_{\dot{\omega}_{\min}}^{\dot{\omega}_{\max}} \left[\underbrace{\frac{\Gamma \hat{\omega} e_y \lambda^T \hat{\mathbf{x}}}{\max(\|\hat{\mathbf{x}}_1\|^2, \epsilon)}}_{=: \delta} \right] \text{ where } f_{aw}(\cdot, \cdot) \text{ as in (24) and } \text{sat}_{\dot{\omega}_{\min}}^{\dot{\omega}_{\max}}[\delta] := \begin{cases} \dot{\omega}_{\max} & , \delta > \dot{\omega}_{\max} \\ \delta & , \dot{\omega}_{\min} \leq \delta \leq \dot{\omega}_{\max} \\ \dot{\omega}_{\min} & , \delta < \dot{\omega}_{\min} \end{cases} \quad (26)$$

which guarantees that (i) the derivative of the estimated angular frequency is bounded, i.e. $\frac{d}{dt}\hat{\omega}(t) \in [\dot{\omega}_{\min}, \dot{\omega}_{\max}]$, and (ii) the estimated angular frequency is positive and bounded from below and above, i.e. $\hat{\omega}(t) \in [\min(\hat{\omega}_0, \omega_{\min}), \max(\hat{\omega}_0, \omega_{\max})]$ for all $t \geq 0$.

IV. IMPLEMENTATION AND MEASUREMENT RESULTS

To validate the proposed algorithms, measurements at a laboratory setup are carried out. The laboratory setup is shown in Fig. 9. For measurements, the voltage is produced by the grid emulator. These voltages are measured by a LEM DVL 500 voltage sensor, analogue-to-digital converted by the dSPACE A/D card DS2004 and internally filtered by a low pass filter with cut-off frequency $\omega_{\text{lpf}} = 5000 \frac{\text{rad}}{\text{s}}$ to suppress high frequency noise. The implementation is done via Matlab/Simulink R2017a on the Host-PC. The executable observers are downloaded via LAN to the dSPACE Processor Board DS1007 and run in real time. The measurement data is captured and analyzed on the Host-PC after the experiment. The implementation data of the conducted measurements is listed in Tab. I.

Three estimation methods are implemented and their estimation performances are compared for the following *two scenarios*:

- (S₁) Estimation of an input signal y with constant fundamental angular frequency (i.e. $\hat{\omega}(t) = \omega(t) = 2\pi 50 \frac{\text{rad}}{\text{s}}$ for all $t \geq 0$) and *ten* harmonics exhibiting amplitude jumps at $t_1 = 0,2\text{s}$, $t_2 = 0,4\text{s}$ and $t_3 = 0,6\text{s}$. The following three estimation methods are implemented and compared:
- parallelized mSOGIs *without* FLL, i.e. observer (13) with \mathbf{l} as in (17);
 - parallelized sSOGIs *without* FLL [7], i.e. observer (13) with $\mathbf{l} = \sqrt{2}\mathbf{c}$ (and $g_\nu = 0$ for all $\nu \in \mathbb{H}_n$); and
 - parallelized Adaptive Notch Filters (ANFs) *without* FLL [4], i.e. observer (13) with $\mathbf{l} = \mathbf{c}$.
- (S₂) Estimation of an input signal y with time-varying fundamental angular frequency $\omega(\cdot)$ (i.e. $\hat{\omega}_0 \neq \omega(0)$) and *ten* harmonics exhibiting frequency jumps at $t_1 = 0,2\text{s}$ and $t_3 = 0,6\text{s}$ and amplitude jumps at $t_2 = 0,4\text{s}$ and $t_3 = 0,6\text{s}$. The following three estimation methods are implemented and compared:



Figure 9: Laboratory setup: (A) Cinergia grid emulator, (B) Host-PC and (C) dSPACE real-time system .

Implementation	
sampling time	$h = 0,1 \text{ ms}$
low-pass filter	$\omega_{\text{lpf}} = 5 \cdot 10^3 \frac{\text{rad}}{\text{s}}$ (for measurements)
parallelized mSOGIs	
observer gains	l as in (17) [$\implies \forall \nu \in \mathbb{H}_\nu: p_{1,2,\nu}^* = -\frac{3}{2} \pm j\nu$]
mFLL	$\Gamma = 60, \varepsilon = 0.1$
Anti-windup	$\omega_{\text{min}} = 39 \frac{\text{rad}}{\text{s}}, \omega_{\text{max}} = 61 \frac{\text{rad}}{\text{s}}$
Rate limitation	$\dot{\omega}_{\text{max}} = 2\pi \times 10 \cdot 10^3 \frac{\text{rad}}{\text{s}}, \dot{\omega}_{\text{min}} = -\dot{\omega}_{\text{max}}$
parallelized sSOGIs [7]	
observer gains	$l = \sqrt{2}c$
sFLL	$\Gamma = 46, \varepsilon = 0.1$ (avoidance of division by zero added)
parallelized ANFs [4]	
filter gains	$l = c$
sFLL (without gain normalization)	$\gamma = 0.5$
Scenario (S₁) with constant fundamental frequency	
initial values of observer (13)	$\hat{x}_0 = \mathbf{0}_{20}$
initial values of sFLL (21) and mFLL (26)	$\hat{\omega}_0 = 2\pi \cdot 50 \frac{\text{rad}}{\text{s}}$ (and $\hat{\omega}(t) = \omega(t)$ for all $t \geq 0$)
Scenario (S₂) with time-varying fundamental frequency	
initial values of observer (13)	$\hat{x}_0 = \mathbf{0}_{20}$
initial values of sFLL (21) and mFLL (26)	$\hat{\omega}_0 = 200 \frac{\text{rad}}{\text{s}} \neq \omega(0) = 2\pi \cdot 50 \frac{\text{rad}}{\text{s}}$

Table I: Implementation and tuning data for simulations and measurements.

- parallelized mSOGIs *with* mFLL, i.e. (13) with l as in (17) and (26);
- parallelized sSOGIs *with* sFLL [7], i.e. observer (13) with $l = \sqrt{2}c$ ($g_\nu = 0$ for all $\nu \in \mathbb{H}_n$) and (21); and
- parallelized ANFs *with* sFLL [4], i.e. observer (13) with $l = c$ and sFLL (20) (without gain normalization⁴).

For both scenarios, the considered input signals y have a significant harmonic distortion. The parameters of the individual harmonics (amplitudes a_ν and frequencies f) of the signal y for Scenario (S₁) and for Scenario (S₂) are collected in Tab. II. Within the considered time interval $[0, 0,8 \text{ s}]$, three jump-like changes in amplitudes and/or fundamental frequency occur at 0,2 s, 0,4 s and 0,6 s. Hence, the input signal and its harmonic content changes abruptly and requires the observers to “restart” their estimation process for each step-like change.

For a fair comparison, all three estimation methods are tuned in such a way that the best feasible estimation performance was achieved within their respective tuning and capability limits. The measurement results for Scenario (S₁) are shown in the

⁴In [4], the gain is ‘ γ ’ and set to 80; the maximal amplitude is $a_1 = 1$. Because the Grid Emulator cannot produce such low voltages and the FLL is driven without a GN, the FLL gain for the ANFs is optimized here with respect to the used amplitudes.

	time interval	parameter	values									
			1	2	3	4	5	6	7	8	9	10
Scenario (S ₁)	0 ≤ t < 0.2s	a _ν /V	194	34	67	46	36	29	29	22	23	19
		f/Hz	50									
	0.2s ≤ t < 0.4s	a _ν /V	145	26	49	35	27	22	22	17	18	15
		f/Hz	50									
	0.4s ≤ t < 0.6s	a _ν /V	216	6	80	38	33	38	0	0	45	17
		f/Hz	50									
	0.6s ≤ t ≤ 0.8s	a _ν /V	193	34	67	47	36	29	30	23	24	19
		f/Hz	50									
Scenario (S ₂)	0 ≤ t < 0.2s	a _ν /V	232	40	80	55	43	63	13	33	6	75
		f/Hz	50									
	0.2s ≤ t < 0.4s	a _ν /V	232	40	80	55	43	62	13	33	6	73
		f/Hz	60									
	0.4s ≤ t < 0.6s	a _ν /V	197	4	73	35	30	36	0	0	41	15
		f/Hz	60									
	0.6s ≤ t ≤ 0.8s	a _ν /V	232	41	80	56	43	63	14	35	8	77
		f/Hz	40									

Table II: Data of considered input signal y for both scenarios (S₁) and (S₂): Amplitudes and frequencies ($f = \frac{\omega}{2\pi}$) of the ten harmonics.

Figures 10, 11 and 12. The results for Scenario (S₂) are depicted in Figures 13, 14 and 15. These results will be discussed in more detail in the next subsections.

A. Discussion of the measurement results obtained for Scenario (S₁)

For Scenario (S₁), the FLL were implemented but the adaption was turned off. Fundamental and estimated angular frequency are identical for this scenario. Therefore, the estimation performances purely according to the respective observer tunings can be compared. The harmonic content of the input signal y undergoes step-like changes at the time instants 0,2s, 0,4s and 0,6s, respectively (see Tab. II and Fig. 10).

Three measurement plots are presented in Figures 10, 11 and 12. The overall estimation performances of the parallelized mSOGIs (—), sSOGIs (—) and ANFs (—) are depicted in Fig. 10: The first, second and third subplots show input signal y (---) & its estimates \hat{y} , the estimation errors $e_y = y - \hat{y}$ and fundamental frequency f (---) & its estimate $\hat{f} = \frac{\hat{\omega}}{2\pi}$, respectively. All three observers are capable of estimating the input signal y . All estimation errors $e_y \rightarrow 0$ tend to zero after a certain time. The parallelized mSOGIs (—) clearly outperform the other two estimation methods in estimation accuracy and estimation speed for all three step-like changes of the input signal y at 0,2s, 0,4s and 0,6s. Estimation is completed in less than 20 ms. This is possibly due to the newly introduced gains g_ν for all $\nu \in \mathbb{H}_n$ which give the necessary degrees of freedom in observer design (recall discussion in Sect. II-C).

In Figures 11 and 12, the estimation performances for the ten individual harmonics are illustrated for the complete time interval $[0, 0,8s]$ of Scenario (S₁) (see Fig. 11) and for the shorter interval $[0,6s, 0,8s]$ (see Zoom in Fig. 12), respectively. In both figures, on the left hand side, the harmonics y_1 to y_{10} (---) and their estimates \hat{y}_1 to \hat{y}_{10} are shown; whereas on the right hand side, the estimation errors $e_1 := y_1 - \hat{y}_1$ to $e_{10} := y_{10} - \hat{y}_{10}$ are depicted. Again, all three estimation methods are capable of tracking the respective harmonic components after a certain time: Amplitudes and phases are estimated correctly with asymptotically vanishing estimation errors. But also for the individual harmonic estimation, the parallelized mSOGIs (—) achieve a much faster estimation performance than the parallelized sSOGIs (—) and the ANFs (—). In particular for the lower harmonics (such as $\nu_1 = 1$, $\nu_2 = 2$, $\nu_3 = 3$ and $\nu_4 = 4$), the estimation is three to four times faster than that of the other two methods.

B. Discussion of the measurement results obtained for Scenario (S₂)

Scenario (S₂) is more challenging. Now, amplitudes and frequency of the input signal y are time-varying. At time instants 0,2s and 0,6s, the fundamental frequency jumps from 50 Hz to 60 Hz and from 60 Hz to 40 Hz, respectively; whereas amplitudes and phases of the harmonic components change abruptly at 0,4s and 0,6s, respectively (see Tab. II and Fig. 10). The measurement results for Scenario (S₂) are plotted in Figures 10, 11 and 12. These figures show the identical quantities as those shown for

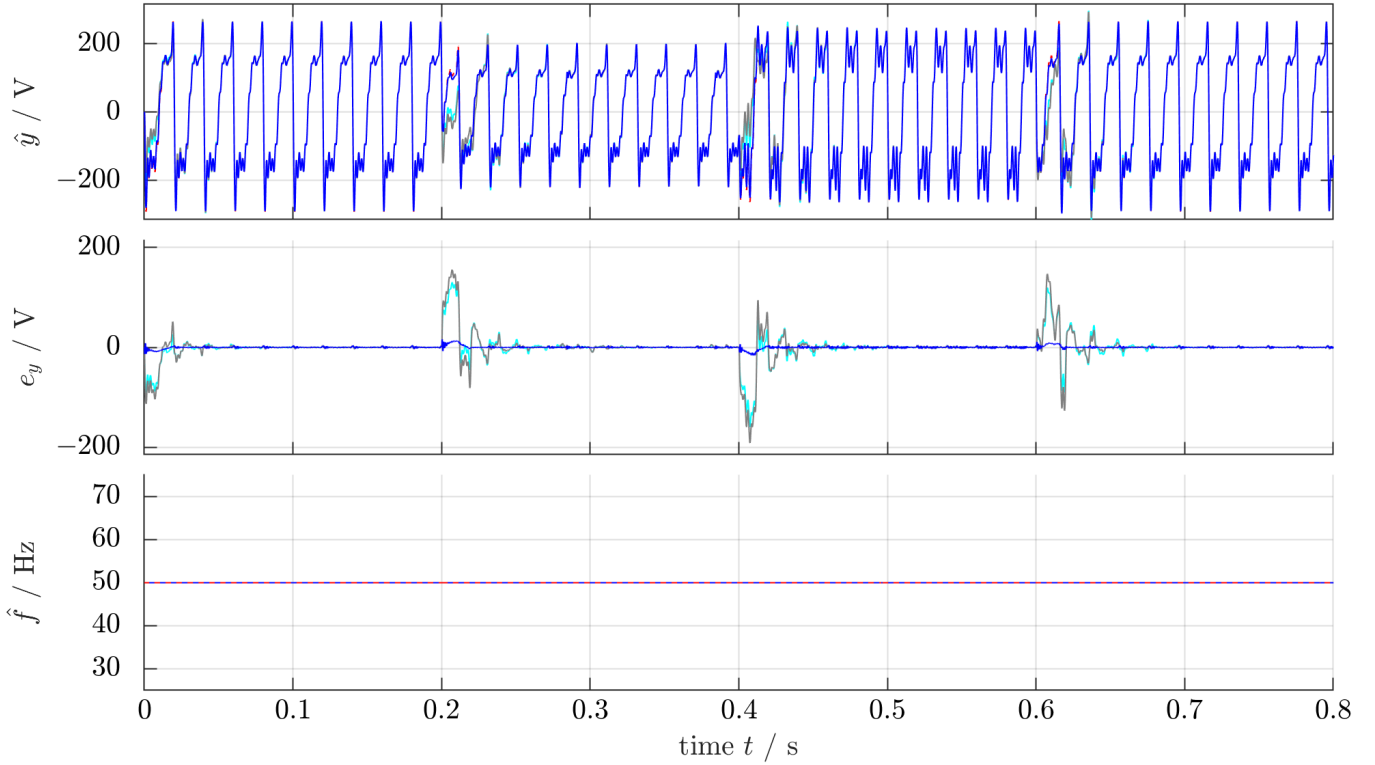


Figure 10: **Measurement results for Scenario (S₁)**: Comparison of the estimation performances of parallelized mSOGIs (—), sSOGIs (—) and ANFs (—) without FLL. Signals shown from top to bottom are: Input signal y (- -) & its estimate \hat{y} ; estimation error $e_y = y - \hat{y}$; frequency $f = \frac{\omega}{2\pi}$ (- -) & its estimate $\hat{f} = \frac{\hat{\omega}}{2\pi}$.

Scenario (S₁).

In Fig. 10, estimated signals \hat{y} , estimation errors $e_y := y - \hat{y}$ and estimated frequencies \hat{f} are shown for the parallelized mSOGIs (—), sSOGIs (—) and ANFs (—), respectively. All three estimation methods are able to correctly estimate the fundamental frequency asymptotically. But, for the parallelized mSOGIs, estimation accuracy and estimation speed of the proposed mFLL are better and the estimation process is much smoother and exhibits less oscillations. Please note that the dip in the frequency estimation of the mFLL after 0,4s does *not* endanger stability of the parallelized mSOGIs (which is due to anti-windup and rate limitation). The overall estimation accuracy of the mSOGIs is very convincing as can be seen in e_y . The estimation error tends to zero within 20 – 40 ms after all three input changes at 0,2s, 0,4s and 0,6s and remains close to zero afterwards. In contrast to that, the overall estimation accuracy and estimation speed of sSOGIs (—) and ANFs (—) are rather bad and slow: Rapid changes in e_y occur for more than 100 ms after each change. Within the last interval [0,6s, 0,8s], the estimation error of both methods does not even tend to zero within 200 ms.

Similar observations can be made by comparing the individual harmonic estimation performances of the three estimation methods as shown in Fig. 11 for the overall time interval [0s, 0,8s] of Scenario (S₂) and in Fig. 12 for the zoomed time interval [0,6s, 0,8s]. Despite the rather bad input estimation performance of parallelized sSOGIs (—) and ANFs (—), their harmonics estimation accuracy is acceptable: All harmonic amplitudes and angles are estimated correctly after some time. However, also here the estimation speed of the parallelized mSOGIs (—) is faster for all harmonic components (see e_1 to e_{10} in Fig. 11). However, the difference in estimation speed is not as significant as it was for Scenario (S₁), which shows that the FLL remains the weakest component of the grid estimation process and has to be improved further (future work).

The last measurement plots depicted in Fig. 15 show the zoomed version of the harmonics estimation during the shorter time interval [0,6s, 0,8s]. Solely, the estimation performance of the parallelized mSOGIs (—) is still acceptable. The estimation accuracies of parallelized sSOGIs (—) and ANFs (—) exhibit significant oscillations and do not tend to zero (in particular for higher harmonics). Their estimation performances are clearly not acceptable anymore. In conclusion, the measurement results obtained for both scenarios have verified the improved performance of the proposed parallelized mSOGIs (—) with mFLL compared to the slower and less accurate estimation performances of parallelized sSOGI (—) and ANFs (—), respectively.

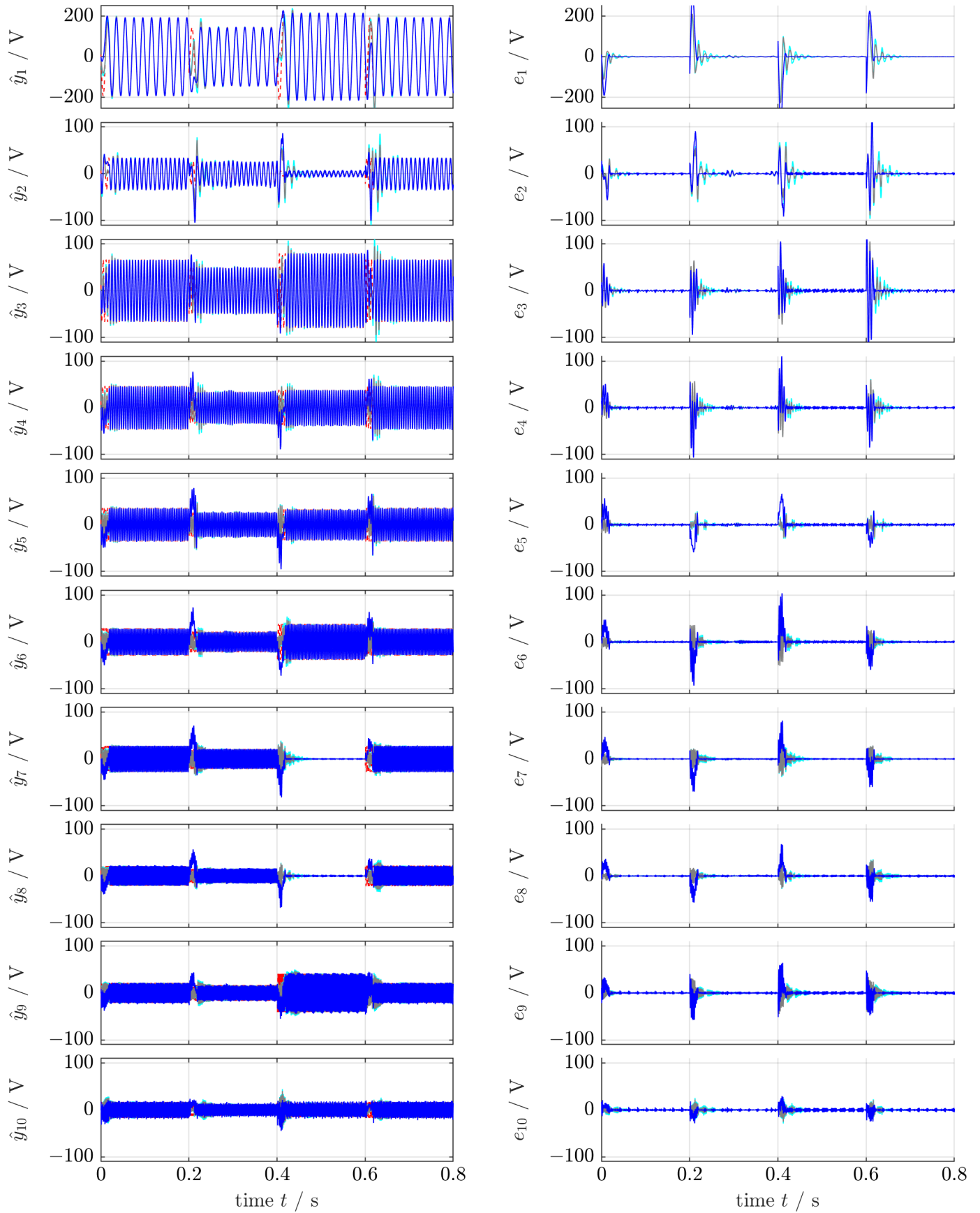


Figure 11: **Measurement results for Scenario (S₁):** Comparison of the estimation performances of parallelized mSOGIs (—), sSOGIs (—) and ANFs (—) without FLL. Signals shown from top to bottom are: Harmonic signals y_1 to y_{10} (- -) & their estimates \hat{y}_1 to \hat{y}_{10} (left) and harmonic estimation errors $e_1 = y_1 - \hat{y}_1$ to $e_{10} = y_{10} - \hat{y}_{10}$ (right).

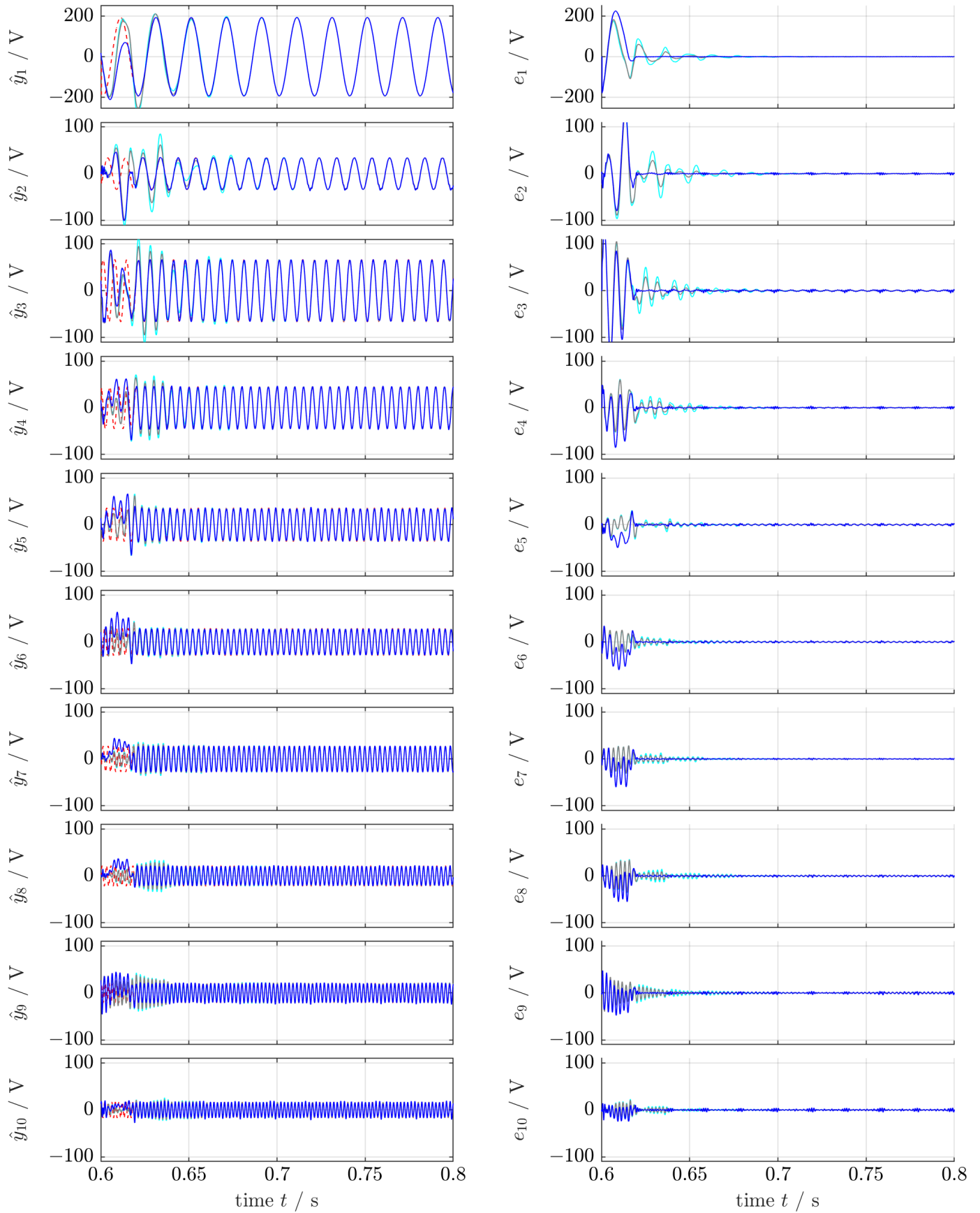


Figure 12: **Measurement results for Scenario (S₁) – Zoom of time interval [0.6s, 0.8s]**: Comparison of the estimation performances of parallelized mSOGIs (—), sSOGIs (—) and ANFs (—) *without* FLL. Signals shown from top to bottom are: Harmonic signals y_1 to y_{10} (- -) & their estimates \hat{y}_1 to \hat{y}_{10} (left) and harmonic estimation errors $e_1 = y_1 - \hat{y}_1$ to $e_{10} = y_{10} - \hat{y}_{10}$ (right).

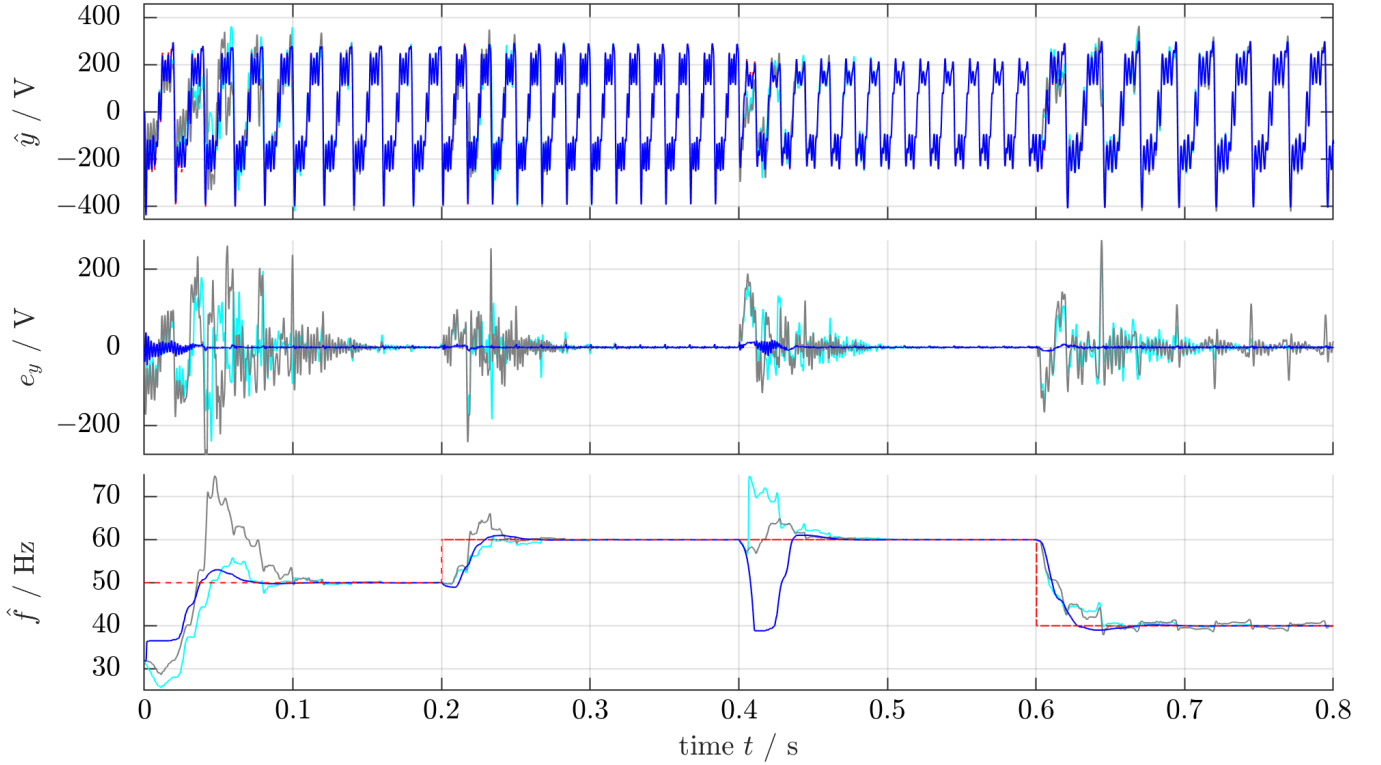


Figure 13: **Measurement results for Scenario (S₂):** Comparison of the estimation performances of parallelized mSOGIs (—), sSOGIs (—) and ANFs (—) with FLL. Signals shown from top to bottom are: Input signal y (---) & its estimate \hat{y} ; estimation error $e_y = y - \hat{y}$; frequency $f = \frac{\omega}{2\pi}$ (---) & its estimate $\hat{f} = \frac{\hat{\omega}}{2\pi}$.

V. CONCLUSION

A modified Second-Order Generalized Integrator (mSOGI) for the ν -th harmonic component and a modified Frequency Locked Loop (mFLL) for the parallelized mSOGIs have been proposed. The number ν can represent any positive not necessarily natural harmonic of an arbitrarily deteriorated input signal for which fundamental and higher harmonic components shall be estimated in real time. In contrast to the ν -th standard SOGI (sSOGI) in literature, the ν -th mSOGI allows (theoretically) for an arbitrarily fast estimation of the in-phase and quadrature signal of any specified harmonic component with prescribed settling time. This is possible due to an additionally introduced feedback gain in the mSOGI design. The proposed mFLL is equipped with sign-correct anti-windup strategy and rate limitation. These modifications enhance the frequency estimation in such a way that the frequency estimate remains positive and bounded and does not change too quickly (independently of mFLL tuning or operating point). Moreover, both enhancements overcome the stability problem of the estimator when a standard FLL (sFLL) is used. Measurement results illustrate and verify the improved estimation performance of the parallelized mSOGIs with and without mFLL in comparison to parallelized sSOGIs and ANFs with and without sFLL.

Future work will focus on (i) further improvements of the mFLL (acceleration of frequency estimation and global stability analysis), (ii) the extension of the presented results to three-phase signals (including DC offsets) and (iii) the real-time estimation of positive, negative and zero sequences of each harmonic component.

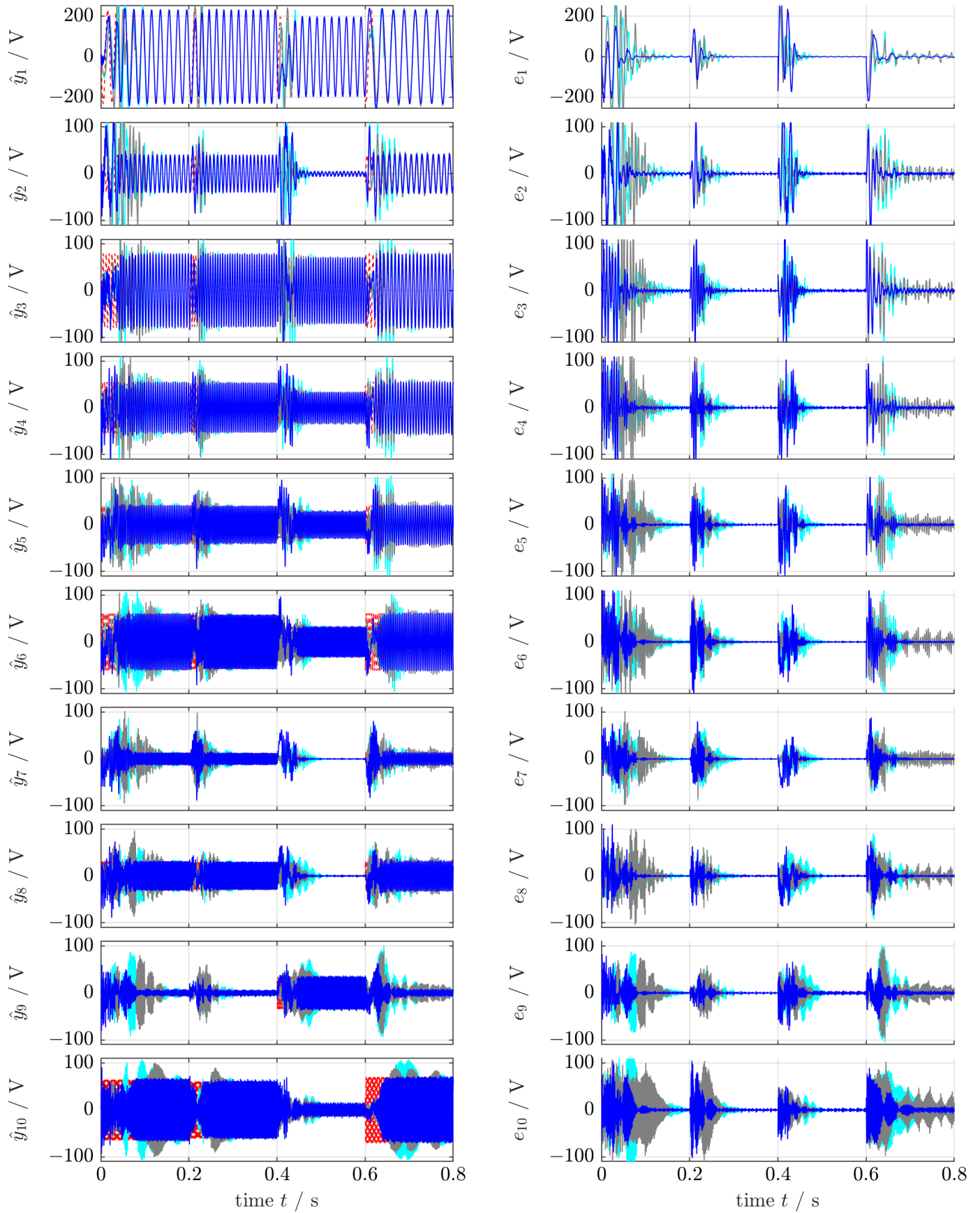


Figure 14: **Measurement results for Scenario (S₂):** Comparison of the estimation performances of parallelized mSOGIs (—), sSOGIs (—) and ANFs (—) with FLL. Signals shown from top to bottom are: Harmonic signals y_1 to y_{10} (- -) & their estimates \hat{y}_1 to \hat{y}_{10} (left) and harmonic estimation errors $e_1 = y_1 - \hat{y}_1$ to $e_{10} = y_{10} - \hat{y}_{10}$ (right).

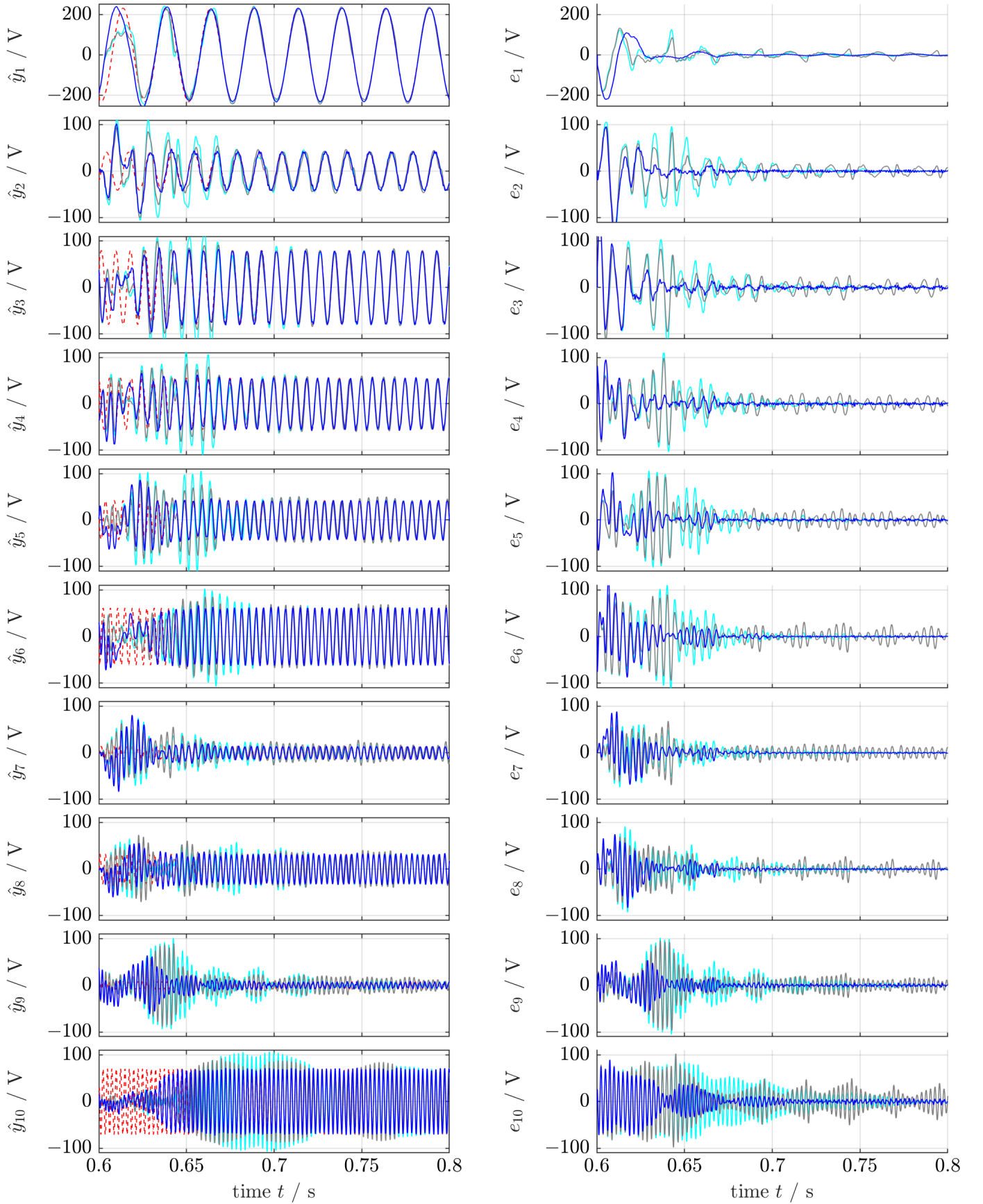


Figure 15: Measurement results for Scenario (S₂) - Zoom of time interval [0.6s, 0.8s]: Comparison of the estimation performances of parallelized mSOGIs (—), sSOGIs (—) and ANFs (—) with FLL. Signals shown from top to bottom are: Harmonic signals y_1 to y_{10} (red dashed lines) & their estimates \hat{y}_1 to \hat{y}_{10} (left) and harmonic estimation errors $e_1 = y_1 - \hat{y}_1$ to $e_{10} = y_{10} - \hat{y}_{10}$ (right).

APPENDIX

In the following appendices, observability and stability of the parallelized SOGIs, the pole placement algorithm and the generalization of the adaption law of the modified FLL for the parallelized mSOGIs are discussed in more detail.

A. Recapitulation

Recall that, any exogenous sinusoidal signal of the form

$$y(t) := \sum_{\nu \in \mathbb{H}_n} \underbrace{a_\nu(t) \cos(\phi_\nu(t))}_{=: y_\nu(t)} \quad \text{where} \quad \mathbb{H}_n := \{1, \nu_2, \dots, \nu_n\}, \quad \nu_i \neq \nu_j \quad \text{for all} \quad i \neq j \in \{1, \dots, n\}$$

can be reduplicated by the parallelization of n sinusoidal internal models [33, Chapter 20]. The overall internal model dynamics are given by

$$\left. \begin{aligned} \frac{d}{dt} \mathbf{x}(t) &= \omega(t) \mathbf{J} \mathbf{x}(t), & \mathbf{x}(0) &= \mathbf{x}_0 \neq \mathbf{0}_{2n} \in \mathbb{R}^{2n} \\ y(t) &= \underbrace{(1, 0, 1, 0, \dots, 1, 0)}_{=: \mathbf{c}^\top \in \mathbb{R}^{2n}} \mathbf{x}(t) \end{aligned} \right\} \quad (27)$$

where $\omega(\cdot) \in \mathcal{C}^{\text{PW}} \cap \mathcal{L}^\infty(\mathbb{R}_{\geq 0}; [\epsilon_\omega, \infty))$ (with $\epsilon_\omega > 0$) and

$$\mathbf{x} := \underbrace{((x_1^\alpha, x_1^\beta), \dots, \mathbf{x}_n^\top)^\top}_{=: \mathbf{x}_1^\top}, \quad \mathbf{J} := \text{blockdiag}(\bar{\mathbf{J}}, \nu_2 \bar{\mathbf{J}}, \dots, \nu_n \bar{\mathbf{J}}) \in \mathbb{R}^{2n \times 2n} \quad \text{and} \quad \bar{\mathbf{J}} = \begin{bmatrix} 0 & -1 \\ 1 & 0 \end{bmatrix} = -\bar{\mathbf{J}}^\top = -\bar{\mathbf{J}}^{-1}. \quad (28)$$

The initial values of the internal model in (27) allow to determine amplitude a_ν and angle ϕ_ν of the ν -th harmonic component.

The overall observer (estimator) consists of the parallelized mSOGIs, i.e. the parallelized internal model (27) with feedback of the input signal $y(\cdot)$ and using the estimated angular frequency $\hat{\omega}(\cdot)$ instead of $\omega(\cdot)$. Its dynamics are given by

$$\left. \begin{aligned} \frac{d}{dt} \hat{\mathbf{x}}(t) &= \hat{\omega}(t) \underbrace{[\mathbf{J} - \mathbf{l} \mathbf{c}^\top]}_{=: \mathbf{A}} \hat{\mathbf{x}}(t) + \hat{\omega}(t) \mathbf{l} y(t), & \hat{\mathbf{x}}(t) &= \hat{\mathbf{x}}_0 \in \mathbb{R}^{2n} \\ \hat{y}(t) &= \mathbf{c}^\top \hat{\mathbf{x}}(t), \end{aligned} \right\} \quad (29)$$

with observer state vector $\hat{\mathbf{x}} := (\hat{\mathbf{x}}_1^\top, \hat{\mathbf{x}}_{\nu_2}^\top, \dots, \hat{\mathbf{x}}_{\nu_n}^\top)^\top \in \mathbb{R}^{2n}$ and observer gain vector $\mathbf{l} := (\mathbf{l}_1^\top, \mathbf{l}_{\nu_2}^\top, \dots, \mathbf{l}_{\nu_n}^\top)^\top \in \mathbb{R}^{2n}$.

B. Observability of the parallelized internal models (27) (for constant $\hat{\omega}$)

The grid state estimation algorithm is based on the idea of observability. The input signal can be considered to be generated by a parallelization of internal models which are individually capable of reduplicating a sinusoidal signal each (representing one harmonic component each). Hence, if this system is observable, an observer can be designed for grid state estimation.

Proposition A.1 (Observability of the linear generating system). *For constant $\omega > 0$ and differing harmonics, i.e. $\nu_i \neq \nu_j$ for all $i \neq j \in \{1, \dots, n\}$, generating system (27) is completely state observable.*

Proof. Note that the following two identities hold

$$\forall k \in \mathbb{N}: \quad \mathbf{J}^k = \text{blockdiag}(\bar{\mathbf{J}}^k, \nu_2^k \bar{\mathbf{J}}^k, \dots, \nu_n^k \bar{\mathbf{J}}^k) \in \mathbb{R}^{2n \times 2n} \quad \text{and} \quad \bar{\mathbf{J}}^k = -\bar{\mathbf{J}}^{k-2} \in \mathbb{R}^{2 \times 2},$$

which imply

$$\text{rank} \begin{bmatrix} \mathbf{c}^\top \\ \mathbf{c}^\top \mathbf{J} \\ \mathbf{c}^\top \mathbf{J}^2 \\ \mathbf{c}^\top \mathbf{J}^3 \\ \vdots \\ \mathbf{c}^\top \mathbf{J}^{2n-2} \\ \mathbf{c}^\top \mathbf{J}^{2n-1} \end{bmatrix} = \text{rank} \begin{bmatrix} 1 & 0 & 1 & 0 & \dots & 1 & 0 \\ 0 & -1 & 0 & -\nu_2 & \dots & 0 & -\nu_n \\ -1 & 0 & -\nu_2^2 & 0 & \dots & -\nu_n^2 & 0 \\ 0 & 1 & 0 & \nu_2^3 & \dots & 0 & \nu_n^3 \\ \vdots & & & \vdots & & & \vdots \\ (-1)^{n-1} & 0 & (-1)^{n-1} \nu_2^{2n-2} & 0 & \dots & (-1)^{n-1} \nu_n^{2n-2} & 0 \\ 0 & (-1)^n & 0 & (-1)^n \nu_2^{2n-1} & \dots & 0 & (-1)^n \nu_n^{2n-1} \end{bmatrix} = 2n. \quad (30)$$

Hence, the pair $(\mathbf{J}, \mathbf{c}^\top)$ is observable [35, Corollary 12.3.19]. □

C. Bounded-input bounded-state/bounded-output stability of the nonlinear observer

As first step, it is shown that for any essentially bounded input signal $y(\cdot)$ and any essentially bounded and strictly positive estimated angular frequency $\hat{\omega}(\cdot)$ the parallelized mSOGIs are bounded-input bounded-state/bounded-output state stable. In other words, the estimated states $\hat{\mathbf{x}}(\cdot)$ and the estimated output $\hat{y}(\cdot)$ will *not* diverge.

Theorem A.2 (Bounded-input bounded-state/bounded-output stability of the dynamics of the parallelized SOGIs). *Consider an essentially bounded input signal $y(\cdot) \in \mathcal{L}^\infty(\mathbb{R}_{\geq 0}; \mathbb{R})$ and assume that (i) the estimated time-varying fundamental angular frequency is continuous, bounded and uniformly bounded away from zero, i.e. $\hat{\omega}(\cdot) \in \mathcal{C}(\mathbb{R}_{\geq 0}; \mathbb{R}_{> 0}) \cap \mathcal{L}^\infty(\mathbb{R}_{\geq 0}; \mathbb{R}_{> 0})$ with $\hat{\omega}(t) \geq \epsilon_\omega > 0$ for all $t \geq 0$, and (ii) the matrix $\mathbf{A} = \mathbf{J} - \mathbf{l}\mathbf{c}^\top$ in (29) is a Hurwitz matrix. Then, the time-varying system (29) is bounded-input bounded-state/bounded-output stable, i.e.*

$$\forall t \geq 0 \exists c_x, c_y > 0: \quad \|\hat{\mathbf{x}}(t)\| \leq c_x \quad \text{and} \quad |\hat{y}(t)| \leq c_y.$$

Proof. First note that, since \mathbf{A} is Hurwitz, there exists $\mathbf{P} = \mathbf{P}^\top > 0$ such that, for any given $\mathbf{Q} = \mathbf{Q}^\top > 0$, the following identity holds [31, Corollary 3.3.47]

$$\mathbf{A}^\top \mathbf{P} + \mathbf{P} \mathbf{A} = -\mathbf{Q}. \quad (31)$$

Moreover, note that

$$\forall a, b \in \mathbb{R} \forall m > 0: \quad 2ab = \frac{a^2}{m} + mb^2 - \left(\frac{a}{\sqrt{m}} - \sqrt{m}b\right)^2 \leq \frac{a^2}{m} + mb^2. \quad (32)$$

Next, introduce the non-negative Lyapunov-like function

$$V: \mathbb{R}^{2n} \rightarrow \mathbb{R}_{\geq 0}, \quad \hat{\mathbf{x}} \mapsto V(\hat{\mathbf{x}}) := \hat{\mathbf{x}}^\top \mathbf{P} \hat{\mathbf{x}}$$

and denote minimal and maximal eigenvalue of \mathbf{P} by $\lambda_{\min}(\mathbf{P})$ and $\lambda_{\max}(\mathbf{P})$, respectively. Then, clearly, the following holds

$$\forall \hat{\mathbf{x}} \in \mathbb{R}^{2n}: \quad \lambda_{\min}(\mathbf{P}) \|\hat{\mathbf{x}}\|^2 \leq V(\hat{\mathbf{x}}) \leq \lambda_{\max}(\mathbf{P}) \|\hat{\mathbf{x}}\|^2 \implies -\|\hat{\mathbf{x}}\|^2 \leq -\frac{1}{\lambda_{\max}(\mathbf{P})} V(\hat{\mathbf{x}}). \quad (33)$$

The right-hand side of (29) is locally Lipschitz continuous with bounded Lipschitz constant and bounded exogenous perturbation. Hence, the solution of (29) exists globally on $\mathbb{R}_{\geq 0}$ [31, Theorem 2.2.14 & Proposition 2.2.19] (but still might diverge as $t \rightarrow \infty$). The time derivative of $V(\cdot)$ along the solution of (29) is, for all $t \geq 0$, given and upper bounded by

$$\begin{aligned} \frac{d}{dt} V(\hat{\mathbf{x}}(t)) &= \frac{d}{dt} \hat{\mathbf{x}}(t)^\top \mathbf{P} \hat{\mathbf{x}}(t) + \hat{\mathbf{x}}(t)^\top \mathbf{P} \frac{d}{dt} \hat{\mathbf{x}}(t) \\ &\stackrel{(29)}{=} \hat{\omega}(t) \left[\hat{\mathbf{x}}(t)^\top (\mathbf{A}^\top \mathbf{P} + \mathbf{P} \mathbf{A}) \hat{\mathbf{x}}(t) + y(t) \mathbf{l}^\top \mathbf{P} \hat{\mathbf{x}}(t) + \hat{\mathbf{x}}(t)^\top \mathbf{P} \mathbf{l} y(t) \right] \\ &= \hat{\omega}(t) \left[\hat{\mathbf{x}}(t)^\top (\mathbf{A}^\top \mathbf{P} + \mathbf{P} \mathbf{A}) \hat{\mathbf{x}}(t) + 2\hat{\mathbf{x}}(t)^\top \mathbf{P} \mathbf{l} y(t) \right] \\ &\stackrel{(31)}{=} \hat{\omega}(t) \left[-\hat{\mathbf{x}}(t)^\top \mathbf{Q} \hat{\mathbf{x}}(t) + 2\hat{\mathbf{x}}(t)^\top \mathbf{P} \mathbf{l} y(t) \right] \\ &\stackrel{(33)}{\leq} \hat{\omega}(t) \left[-\lambda_{\min}(\mathbf{Q}) \|\hat{\mathbf{x}}(t)\|^2 + 2 \underbrace{\|\hat{\mathbf{x}}(t)\|}_{=:a} \underbrace{\|\mathbf{P}\| \|\mathbf{l}\| \|y\|_\infty}_{=:b} \right] \\ &\stackrel{(32)}{\leq} \hat{\omega}(t) \left[-\underbrace{\left(\lambda_{\min}(\mathbf{Q}) - \frac{1}{m} \right)}_{\exists m \geq 1 \text{ s.t. } (\cdot) \geq \epsilon_m > 0} \|\hat{\mathbf{x}}(t)\|^2 + \underbrace{m \|\mathbf{P}\|^2 \|\mathbf{l}\|^2 \|y\|_\infty^2}_{=:c_m < \infty} \right] \\ &\stackrel{(33)}{\leq} \left[-\frac{\epsilon_m \epsilon_\omega}{\lambda_{\max}(\mathbf{P})} V(\hat{\mathbf{x}}(t)) + c_m \|\hat{\omega}\|_\infty \right] \\ \implies V(\hat{\mathbf{x}}(t)) &\leq V(\hat{\mathbf{x}}(0)) + c_m \|\hat{\omega}\|_\infty \frac{\lambda_{\max}(\mathbf{P})}{\epsilon_m \epsilon_\omega}, \end{aligned} \quad (34)$$

where, in the last step, the Bellman-Gronwall Lemma [36, p. 102f.] was used in its differential form (see Lemma 5.50 and Example 5.51 in [33]). Hence, in view of (33) and (34), and with c as in (27), one can conclude that

$$\forall t \geq 0: \|\hat{\mathbf{x}}(t)\| \stackrel{(33),(34)}{\leq} \sqrt{\frac{1}{\lambda_{\min}(\mathbf{P})} \left(V(\hat{\mathbf{x}}(0)) + c_m \|\hat{\omega}\|_\infty \frac{\lambda_{\max}(\mathbf{P})}{\epsilon_m \epsilon_\omega} \right)} =: c_x < \infty$$

$$\text{and} \quad |\hat{y}(t)| \stackrel{(29)}{\leq} \|\mathbf{c}\| \|\hat{\mathbf{x}}(t)\| \leq \|\mathbf{c}\| c_x =: c_y < \infty,$$

which completes the proof. \square

D. Boundedness and exponential decay of the signal estimation error

It is shown that, for piecewise continuous (sinusoidal) and bounded input signals $y(\cdot) \in \mathcal{C}^{\text{pw}}(\mathbb{R}_{\geq 0}; \mathbb{R}) \cap \mathcal{L}^\infty(\mathbb{R}_{\geq 0}; \mathbb{R})$, the estimation error of the parallelized mSOGIs (or sSOGIs) is bounded. Additionally, if the piecewise constant fundamental angular frequency $\omega(\cdot)$ is correctly estimated, the estimation error decays exponentially.

To present the result, an important observation must be introduced. Note that, for $\omega(\cdot) \in \mathcal{C}^{pw} \cap \mathcal{L}^\infty(\mathbb{R}_{\geq 0}; [\epsilon_\omega, \infty))$, any piecewise continuous (sinusoidal-like) signal of the form $y(\cdot) = \sum_{\nu \in \mathbb{H}_n} a_\nu \cos(\nu \int_0^\cdot \omega(\tau) d\tau + \phi_{0,\nu})$ on any bounded interval $\mathbb{I}_i := [t_i, t_{i+1})$, $i \in \mathbb{N}_0$ (such that $\mathbb{R}_{\geq 0} = \mathbb{I}_0 \cup \mathbb{I}_1 \cup \mathbb{I}_2 \cup \dots$) can be generated by (the output of) a properly initialized internal model [37] of the following form

$$\left. \begin{aligned} \forall t \in \mathbb{I}_i: \quad \frac{d}{dt} \mathbf{x}(t) &= \omega(t) \mathbf{J} \mathbf{x}(t), & \mathbf{x}(t_i) &= \mathbf{x}_{i,0} \in \mathbb{R}^{2n} \\ y(t) &= \mathbf{c}^\top \mathbf{x}(t) \end{aligned} \right\} \quad (35)$$

with \mathbf{J} as in (28). $\omega(\cdot)$ can be considered as an external input to the internal model. Clearly, for any real (finite) initial value $\mathbf{x}_{i,0} \in \mathbb{R}^{2n}$ for the i -th time interval \mathbb{I}_i , all states of the internal model (35) are essentially bounded, i.e. $\mathbf{x}(\cdot) \in \mathcal{L}^\infty(\mathbb{R}_{\geq 0}; \mathbb{R}^{2n})$. Note that $\omega(\cdot)$, $\phi_{0,\nu}$ and a_ν for all $\nu \in \mathbb{H}_n$ might change for each interval \mathbb{I}_i . Now, the result can be stated.

Theorem A.3 (Boundedness and exponential decay of the signal estimation error). *Let $\epsilon_\omega > 0$, $\mathbb{H}_n = \{\nu_1, \nu_2, \dots, \nu_n\}$, $a_\nu \geq 0$, $\phi_{0,\nu}$ for all $\nu \in \mathbb{H}_n$ and $\hat{\omega}(\cdot), \omega(\cdot) \in \mathcal{C}^{pw} \cap \mathcal{L}^\infty(\mathbb{R}_{\geq 0}; [\epsilon_\omega, \infty))$. Consider any piecewise continuous and bounded input signals, i.e. $y(\cdot) = \sum_{\nu \in \mathbb{H}_n} a_\nu \cos(\nu \int_0^\cdot \omega(\tau) d\tau + \phi_{0,\nu}) \in \mathcal{C}^{pw} \cap \mathcal{L}^\infty(\mathbb{R}_{\geq 0}; \mathbb{R})$ on any bounded interval $\mathbb{I}_i := [t_i, t_{i+1})$, $i \in \mathbb{N}_0$ (such that $\mathbb{R}_{\geq 0} = \mathbb{I}_0 \cup \mathbb{I}_1 \cup \mathbb{I}_2 \cup \dots$), generated by the internal model (35) and assume that $y(\cdot)$ is fed to the parallelized SOGI system (29) with $\mathbf{A} := \mathbf{J} - \mathbf{l}\mathbf{c}^\top$ being a Hurwitz matrix. Then, the estimation error, defined by*

$$\mathbf{e}_x(t) := \mathbf{x}(t) - \hat{\mathbf{x}}(t) \in \mathbb{R}^{2n} \quad (36)$$

with $\mathbf{x}(t)$ as in (35) and $\hat{\mathbf{x}}(t)$ as in (29), is bounded, i.e. there exists $c_e > 0$ such that $\|\mathbf{e}_x(t)\| \leq c_e$ for all $t \geq 0$. Moreover, if, for some $i \in \mathbb{N}_0$, $\omega(t) = \hat{\omega}(t)$ for all $t \in \mathbb{I}_{ss} \subseteq \mathbb{I}_i$, then the norm of the estimation error is exponentially decaying, i.e. there exist constants $c_V, \mu_V > 0$ such that $\|\mathbf{e}_x(t)\| \leq c_V \|\mathbf{e}_x(t_i)\| e^{-\mu_V(t-t_i)}$ for all $t \in \mathbb{I}_{ss}$.

Proof. Note that, for any interval \mathbb{I}_i , combining (29) and (35) yields

$$\forall t \in \mathbb{I}_i: \quad \underbrace{\frac{d}{dt} \begin{pmatrix} \hat{\mathbf{x}}(t) \\ \mathbf{x}(t) \end{pmatrix}}_{\in \mathbb{R}^{4n}} = \begin{bmatrix} \hat{\omega}(t) \mathbf{A} & \hat{\omega}(t) \mathbf{l}\mathbf{c}^\top \\ \mathbf{O}_{2n \times 2n} & \omega(t) \mathbf{J} \end{bmatrix} \begin{pmatrix} \hat{\mathbf{x}}(t) \\ \mathbf{x}(t) \end{pmatrix}, \quad \begin{pmatrix} \hat{\mathbf{x}}(t_i) \\ \mathbf{x}(t_i) \end{pmatrix} = \begin{pmatrix} \hat{\mathbf{x}}_{i,0} \\ \mathbf{x}_{i,0} \end{pmatrix} \in \mathbb{R}^{4n}. \quad (37)$$

Next, introduce the angular frequency estimation error

$$\forall t \in \mathbb{I}_i: \quad e_\omega(t) := \omega(t) - \hat{\omega}(t) \iff \omega(t) = e_\omega(t) + \hat{\omega}(t), \quad (38)$$

and evaluate the time derivative of the estimation error vector as follows

$$\begin{aligned} \forall t \in \mathbb{I}_i: \quad \underbrace{\frac{d}{dt} (\mathbf{x}(t) - \hat{\mathbf{x}}(t))}_{\stackrel{(36)}{=} \mathbf{e}_x(t)} &= \begin{bmatrix} -\mathbf{I}_{2n} & \mathbf{I}_{2n} \end{bmatrix} \frac{d}{dt} \begin{pmatrix} \hat{\mathbf{x}}(t) \\ \mathbf{x}(t) \end{pmatrix} \\ &\stackrel{(37)}{=} -\hat{\omega}(t) \mathbf{A} \hat{\mathbf{x}}(t) - (\hat{\omega}(t) \mathbf{l}\mathbf{c}^\top - \omega(t) \mathbf{J}) \mathbf{x}(t) \\ &\stackrel{(38)}{=} -\hat{\omega}(t) \mathbf{A} \hat{\mathbf{x}}(t) - \hat{\omega}(t) \underbrace{(\mathbf{l}\mathbf{c}^\top - \mathbf{J})}_{\stackrel{(29)}{=} -\mathbf{A}}} \mathbf{x}(t) + e_\omega(t) \mathbf{J} \mathbf{x}(t) \\ &= \hat{\omega}(t) \mathbf{A} \mathbf{e}_x(t) + e_\omega(t) \mathbf{J} \mathbf{x}(t). \end{aligned} \quad (39)$$

Now, the time derivative of the Lyapunov-like function $V(\mathbf{e}_x(\cdot)) = \mathbf{e}_x(\cdot)^\top \mathbf{P} \mathbf{e}_x(\cdot)$ (with \mathbf{P} as introduced in (31)) is given for all $t \in \mathbb{I}_i = [t_i, t_{i+1})$, along the solution of (39), as follows

$$\begin{aligned} \frac{d}{dt} V(\mathbf{e}_x(t)) &= \frac{d}{dt} \mathbf{e}_x(t)^\top \mathbf{P} \mathbf{e}_x(t) + \mathbf{e}_x(t)^\top \mathbf{P} \frac{d}{dt} \mathbf{e}_x(t) \\ &\stackrel{(39)}{=} \hat{\omega}(t) \mathbf{e}_x(t)^\top (\mathbf{A}^\top \mathbf{P} + \mathbf{P} \mathbf{A}) \mathbf{e}_x(t) + e_\omega(t) (\mathbf{e}_x(t)^\top \mathbf{P} \mathbf{J} \mathbf{x}(t) + \mathbf{x}(t)^\top \mathbf{J}^\top \mathbf{P} \mathbf{e}_x(t)) \\ &= \hat{\omega}(t) \mathbf{e}_x(t)^\top (\mathbf{A}^\top \mathbf{P} + \mathbf{P} \mathbf{A}) \mathbf{e}_x(t) + 2e_\omega(t) \mathbf{e}_x(t)^\top \mathbf{P} \mathbf{J} \mathbf{x}(t) \\ &\stackrel{(31)}{=} -\hat{\omega}(t) \mathbf{e}_x(t)^\top \mathbf{Q} \mathbf{e}_x(t) + 2e_\omega(t) \mathbf{e}_x(t)^\top \mathbf{P} \mathbf{J} \mathbf{x}(t) \\ &\stackrel{(33)}{\leq} -\hat{\omega}(t) \lambda_{\min}(\mathbf{Q}) \|\mathbf{e}_x(t)\|^2 + 2 \underbrace{\sqrt{\hat{\omega}(t)} \|\mathbf{e}_x(t)\|}_{=:a} \underbrace{|e_\omega(t)| \|\mathbf{P}\| \|\mathbf{J}\| \|\mathbf{x}\|_\infty \frac{1}{\sqrt{\hat{\omega}(t)}}}_{=:b} \\ &\stackrel{(32)}{\leq} -\hat{\omega}(t) \left(\underbrace{\lambda_{\min}(\mathbf{Q}) - \frac{1}{m}}_{\exists m \geq 1 \text{ s.t. } (\cdot) \geq \epsilon'_m > 0} \right) \|\mathbf{e}_x(t)\|^2 + e_\omega(t)^2 \underbrace{\frac{m}{\epsilon_\omega} \|\mathbf{P}\|^2 \|\mathbf{J}\|^2 \|\mathbf{x}\|_\infty^2}_{=:c'_m < \infty} \end{aligned}$$

$$\begin{aligned}
&\stackrel{(33)}{\leq} - \underbrace{\frac{\epsilon'_m \epsilon_\omega}{\lambda_{\max}(\mathbf{P})}}_{=:\mu_V > 0} V(\mathbf{e}_x(t)) + e_\omega(t)^2 c'_m \\
\implies V(\mathbf{e}_x(t)) &\leq V(\mathbf{e}_x(t_i)) e^{-\mu_V(t-t_i)} + c'_m \int_{t_i}^t e_\omega(\tau)^2 e^{-\mu_V(t-\tau)} d\tau,
\end{aligned} \tag{40}$$

where, in the last step, the Bellman-Gronwall Lemma in its differential form (see Lemma 5.50 and Example 5.51 in [33]) was used again. Note that $e_\omega(\cdot) \in \mathcal{L}^\infty(\mathbb{R}_{\geq 0}; \mathbb{R})$, since $\widehat{\omega}(\cdot)$, $\omega(\cdot) \in \mathcal{L}^\infty(\mathbb{R}_{\geq 0}; [\epsilon_\omega, \infty))$ on each interval \mathbb{I}_i . Hence,

$$\begin{aligned}
\forall t \in \mathbb{I}_i: \quad \|\mathbf{e}_x(t)\|^2 &\stackrel{(33),(40)}{\leq} \frac{1}{\lambda_{\min}(\mathbf{P})} \left[V(\mathbf{e}_x(t_i)) e^{-\mu_V(t-t_i)} + c'_m \int_{t_i}^t e_\omega(\tau)^2 e^{-\mu_V(t-\tau)} d\tau \right], \\
&\stackrel{(33)}{\leq} \frac{\lambda_{\max}(\mathbf{P})}{\lambda_{\min}(\mathbf{P})} \|\mathbf{e}_x(t_i)\| e^{-\mu_V(t-t_i)} + \frac{c'_m}{\lambda_{\min}(\mathbf{P})} \int_{t_i}^t e_\omega(\tau)^2 e^{-\mu_V(t-\tau)} d\tau,
\end{aligned} \tag{41}$$

and, clearly, for all $t \in \mathbb{I}_{ss} \subset \mathbb{I}_i$ where $e_\omega(t) = 0$, the estimation error is exponentially decaying. This completes the proof. \square

Remark A.4 (Exponential stability and input-to-state stability). *Note that, if $e_\omega(t) = 0$ for all $t \geq t_i$ for some $t_i \geq 0$ and $i \in \mathbb{N}_0$, (41) gives exponential stability and, hence, asymptotic estimation (tracking), i.e. $\lim_{t \rightarrow \infty} \|\mathbf{e}_x(t)\| = \mathbf{0}_{2n}$ which implies $\lim_{t \rightarrow \infty} |y(t) - \widehat{y}(t)| = 0$. Moreover, note that (41) directly implies input-to-state stability (see e.g. Part “Input to State Satbility: Basic Concepts and Results” by E.D. Sontag in [38]).*

E. Pole placement algorithm for the parallelized mSOGIs

Before the main results of this section can be presented, a preliminary observation has to be made. Consider the matrix

$$\forall n \in \mathbb{N}, \forall z_1, \dots, z_n \in \mathbb{C}: \mathbf{S}^{-1} := \begin{bmatrix} \mathbf{R}_1^{-1} & \mathbf{R}_2^{-1} & \dots & \mathbf{R}_n^{-1} \\ \sum_{\substack{i=1 \\ i \neq 1}}^n z_i^2 \mathbf{R}_1^{-1} & \sum_{\substack{i=1 \\ i \neq 2}}^n z_i^2 \mathbf{R}_2^{-1} & \dots & \sum_{\substack{i=1 \\ i \neq n}}^n z_i^2 \mathbf{R}_n^{-1} \\ \vdots & \vdots & \ddots & \vdots \\ \prod_{\substack{i=1 \\ i \neq 1}}^n z_i^2 \mathbf{R}_1^{-1} & \prod_{\substack{i=1 \\ i \neq 2}}^n z_i^2 \mathbf{R}_2^{-1} & \dots & \prod_{\substack{i=1 \\ i \neq n}}^n z_i^2 \mathbf{R}_n^{-1} \end{bmatrix}, \quad \mathbf{R}_i^{-1} = \begin{bmatrix} 1 & 0 \\ 0 & -z_i \end{bmatrix}. \tag{42}$$

Its inverse is given by

$$\mathbf{S} = \begin{bmatrix} \frac{z_1^{2(n-1)}}{\prod_{\substack{i=1 \\ i \neq 1}}^n (z_1^2 - z_i^2)} \mathbf{R}_1 & -\frac{z_1^{2(n-2)}}{\prod_{\substack{i=1 \\ i \neq 1}}^n (z_1^2 - z_i^2)} \mathbf{R}_1 & \dots & \frac{(-1)^{n+1}}{\prod_{\substack{i=1 \\ i \neq 1}}^n (z_1^2 - z_i^2)} \mathbf{R}_1 \\ \frac{z_2^{2(n-1)}}{\prod_{\substack{i=1 \\ i \neq 2}}^n (z_2^2 - z_i^2)} \mathbf{R}_2 & -\frac{z_2^{2(n-2)}}{\prod_{\substack{i=1 \\ i \neq 2}}^n (z_2^2 - z_i^2)} \mathbf{R}_2 & \dots & \frac{(-1)^{n+1}}{\prod_{\substack{i=1 \\ i \neq 2}}^n (z_2^2 - z_i^2)} \mathbf{R}_2 \\ \vdots & \vdots & \ddots & \vdots \\ \frac{z_n^{2(n-1)}}{\prod_{\substack{i=1 \\ i \neq n}}^n (z_n^2 - z_i^2)} \mathbf{R}_n & -\frac{z_n^{2(n-2)}}{\prod_{\substack{i=1 \\ i \neq n}}^n (z_n^2 - z_i^2)} \mathbf{R}_n & \dots & \frac{(-1)^{n+1}}{\prod_{\substack{i=1 \\ i \neq n}}^n (z_n^2 - z_i^2)} \mathbf{R}_n \end{bmatrix}, \tag{43}$$

since the product of the c -th column of \mathbf{S}^{-1} and the r -th row of \mathbf{S} yields

$$\begin{aligned}
&\frac{z_r^{2(n-1)}}{\prod_{\substack{j=1 \\ j \neq r}}^n (z_r^2 - z_j^2)} \mathbf{R}_c \mathbf{R}_r^{-1} - \sum_{\substack{i=1 \\ i \neq c}}^n z_i^2 \frac{z_r^{2(n-2)}}{\prod_{\substack{j=1 \\ j \neq r}}^n (z_r^2 - z_j^2)} \mathbf{R}_c \mathbf{R}_r^{-1} + \dots + \prod_{\substack{i=1 \\ i \neq c}}^n z_i^2 \frac{(-1)^{n+1}}{\prod_{\substack{j=1 \\ j \neq r}}^n (z_r^2 - z_j^2)} \mathbf{R}_c \mathbf{R}_r^{-1} \\
&= \left(z_r^{2(n-1)} - z_r^{2(n-2)} \sum_{\substack{i=1 \\ i \neq c}}^n z_i^2 + \dots + (-1)^{n+1} \prod_{\substack{i=1 \\ i \neq c}}^n z_i^2 \right) \frac{1}{\prod_{\substack{j=1 \\ j \neq r}}^n (z_r^2 - z_j^2)} \mathbf{R}_c \mathbf{R}_r^{-1} = \begin{cases} \mathbf{0}_{2 \times 2}, & c \neq r \\ \mathbf{I}_2, & c = r. \end{cases}
\end{aligned}$$

Now, the main result can be stated.

Proposition A.5 (Pole placement). *Consider the matrix $\mathbf{A} := \mathbf{J} - \mathbf{l}\mathbf{c}^\top$ with \mathbf{J} as in (28) and \mathbf{c} as in (27). If and only if the feedback vector \mathbf{l} is chosen as*

$$\mathbf{l} = \mathbf{S} \widetilde{\mathbf{p}}_{\mathbf{A}}^*, \tag{44}$$

then the desired characteristic polynomial

$$\chi_{\mathbf{A}}^*(s) := \prod_{i=1}^{2n} (s - p_i^*) \quad (45)$$

and characteristic polynomial

$$\chi_{\mathbf{A}}(s) = \prod_{i=1}^n (s^2 + \nu_i^2) - \sum_{i=1}^n g_i \nu_i^2 \prod_{\substack{k=1 \\ k \neq i}}^n (s^2 + \nu_k^2) + s \sum_{i=1}^n k_i \nu_i \prod_{\substack{k=1 \\ k \neq i}}^n (s^2 + \nu_k^2) \quad (46)$$

have identical coefficients and, hence, $\mathbf{A} = \mathbf{J} - \mathbf{l}\mathbf{c}^\top$ is a Hurwitz matrix with eigenvalues $p_i^* \in \mathbb{C}_{<0}$, $i \in \{1, \dots, 2n\}$, as specified in (45).

Proof. For arbitrary k_i and g_i in the feedback gain vector \mathbf{l} as in (44), recall the characteristic polynomial $\chi_{\mathbf{A}}$ given in (46) and collect its coefficients in the following coefficient vector

$$\begin{aligned} \mathbf{p}_{\mathbf{A}} &= \left(\sum_{i=1}^n k_i \nu_i, \sum_{i=1}^n \nu_i^2 - g_i \nu_i^2, \sum_{i=1}^n k_i \nu_i \sum_{\substack{j=1 \\ j \neq i}}^n \nu_j^2, \sum_{i=1}^n \nu_i^2 \sum_{\substack{j=i+1 \\ j \neq i}}^n \nu_j^2 - g_i \nu_i^2 \sum_{\substack{j=1 \\ j \neq i}}^n \nu_j^2, \dots, \sum_{i=1}^n k_i \nu_i \prod_{\substack{j=1 \\ j \neq i}}^n \nu_j^2, \prod_{i=1}^n \nu_i^2 - \sum_{i=1}^n g_i \prod_{j=1}^n \nu_j^2 \right)^\top \\ &= \left(0, \sum_{i=1}^n \nu_i^2, 0, \sum_{i=1}^n \nu_i^2 \sum_{j=i+1}^n \nu_j^2, \dots, 0, \prod_{i=1}^n \nu_i^2 \right)^\top \\ &\quad + \left(\sum_{i=1}^n k_i \nu_i, -\sum_{i=1}^n g_i \nu_i^2, \sum_{i=1}^n k_i \nu_i \sum_{\substack{j=1 \\ j \neq i}}^n \nu_j^2, -\sum_{i=1}^n g_i \nu_i^2 \sum_{\substack{j=1 \\ j \neq i}}^n \nu_j^2, \dots, \sum_{i=1}^n k_i \nu_i \prod_{\substack{j=1 \\ j \neq i}}^n \nu_j^2, -\sum_{i=1}^n g_i \prod_{j=1}^n \nu_j^2 \right)^\top. \end{aligned} \quad (47)$$

A comparison with the desired polynomial in (45), having the coefficient vector

$$\mathbf{p}_{\mathbf{A}}^* := \left(-\sum_{i=1}^{2n} p_i^*, \sum_{i=1}^{2n} p_i^* \sum_{j=i+1}^{2n} p_j^*, -\sum_{i=1}^{2n} p_i^* \sum_{j=i+1}^{2n} p_j^* \sum_{k=j+1}^{2n} p_k^*, \dots, \prod_{i=1}^{2n} p_i^* \right)^\top,$$

leads to the linear system of equations

$$\stackrel{(47)}{\implies} \mathbf{p}_{\mathbf{A}}^* - \begin{pmatrix} 0 \\ \sum_{i=1}^n \nu_i^2 \\ \vdots \\ 0 \\ \prod_{i=1}^n \nu_i^2 \end{pmatrix} = \underbrace{\begin{bmatrix} \mathbf{R}_1^{-1} & \mathbf{R}_2^{-1} & \dots & \mathbf{R}_n^{-1} \\ \sum_{\substack{i=1 \\ i \neq 1}}^n \nu_i^2 \mathbf{R}_1^{-1} & \sum_{\substack{i=1 \\ i \neq 2}}^n \nu_i^2 \mathbf{R}_2^{-1} & \dots & \sum_{\substack{i=1 \\ i \neq n}}^n \nu_i^2 \mathbf{R}_n^{-1} \\ \vdots & \vdots & \ddots & \vdots \\ \prod_{\substack{i=1 \\ i \neq 1}}^n \nu_i^2 \mathbf{R}_1^{-1} & \prod_{\substack{i=1 \\ i \neq 2}}^n \nu_i^2 \mathbf{R}_2^{-1} & \dots & \prod_{\substack{i=1 \\ i \neq n}}^n \nu_i^2 \mathbf{R}_n^{-1} \end{bmatrix}}_{\stackrel{(42)}{=} \mathbf{S}^{-1}} \mathbf{l}, \quad \text{with } \mathbf{R}_i^{-1} = \begin{bmatrix} 1 & 0 \\ 0 & -\nu_i \end{bmatrix}. \quad (48)$$

Inserting \mathbf{l} as in (44) and invoking the preliminary result in (43), one indeed obtains $\mathbf{p}_{\mathbf{A}}^* = \mathbf{p}_{\mathbf{A}}$. Or in other words, the feedback gain vector to achieve pole placement is given by

$$\stackrel{(43)}{\implies} \mathbf{l} = \underbrace{\begin{bmatrix} \frac{\nu_1^{2(n-1)}}{\prod_{\substack{i=1 \\ i \neq 1}}^n (\nu_1^2 - \nu_i^2)} \mathbf{R}_1 & -\frac{\nu_1^{2(n-2)}}{\prod_{\substack{i=1 \\ i \neq 1}}^n (\nu_1^2 - \nu_i^2)} \mathbf{R}_1 & \dots & \frac{(-1)^{n+1}}{\prod_{\substack{i=1 \\ i \neq 1}}^n (\nu_1^2 - \nu_i^2)} \mathbf{R}_1 \\ \frac{\nu_2^{2(n-1)}}{\prod_{\substack{i=1 \\ i \neq 2}}^n (\nu_2^2 - \nu_i^2)} \mathbf{R}_2 & -\frac{\nu_2^{2(n-2)}}{\prod_{\substack{i=1 \\ i \neq 2}}^n (\nu_2^2 - \nu_i^2)} \mathbf{R}_2 & \dots & \frac{(-1)^{n+1}}{\prod_{\substack{i=1 \\ i \neq 2}}^n (\nu_2^2 - \nu_i^2)} \mathbf{R}_2 \\ \vdots & \vdots & \ddots & \vdots \\ \frac{\nu_n^{2(n-1)}}{\prod_{\substack{i=1 \\ i \neq n}}^n (\nu_n^2 - \nu_i^2)} \mathbf{R}_n & -\frac{\nu_n^{2(n-2)}}{\prod_{\substack{i=1 \\ i \neq n}}^n (\nu_n^2 - \nu_i^2)} \mathbf{R}_n & \dots & \frac{(-1)^{n+1}}{\prod_{\substack{i=1 \\ i \neq n}}^n (\nu_n^2 - \nu_i^2)} \mathbf{R}_n \end{bmatrix}}_{=} \mathbf{S} \begin{pmatrix} \mathbf{p}_{\mathbf{A}}^* - \begin{pmatrix} 0 \\ \sum_{i=1}^n \nu_i^2 \\ \vdots \\ 0 \\ \prod_{i=1}^n \nu_i^2 \end{pmatrix} \\ \vdots \\ \vdots \\ \vdots \\ \vdots \end{pmatrix} \Bigg|_{=} \mathbf{p}_{\mathbf{A}}^* \end{pmatrix}. \quad (49)$$

Clearly, if and only if $\mathbf{p}_A^* = \mathbf{p}_A$ holds, the eigenvalues of $\mathbf{A} = \mathbf{J} - \mathbf{l}c^\top$ are given by $p_i^* \in \mathbb{C}_{<0}$, $i \in \{1, \dots, 2n\}$, as specified in (45) and \mathbf{A} is a Hurwitz matrix. This completes the proof. \square

F. Generalization of the adaptation law of the mFLL for the parallelized mSOGIs

1) *Preliminaries:* To ease the understanding of the following derivations, preliminary calculations are introduced.

First, consider a stable transfer function in the frequency domain, given by

$$\mathcal{G}(j\omega) := \frac{n(\omega)}{d(\omega)} = \frac{\Re(n(\omega)) + j\Im(n(\omega))}{\Re(d(\omega)) + j\Im(d(\omega))} = \frac{\Re(n(\omega))\Re(d(\omega)) + \Im(n(\omega))\Im(d(\omega))}{\Re^2(d(\omega)) + \Im^2(d(\omega))} + j \frac{\Re(d(\omega))\Im(n(\omega)) - \Re(n(\omega))\Im(d(\omega))}{\Re^2(d(\omega)) + \Im^2(d(\omega))}.$$

Its amplitude and phase responses are given by

$$A_{\mathcal{G}}(\omega) = \sqrt{\frac{\Re^2(n(\omega)) + \Im^2(n(\omega))}{\Re^2(d(\omega)) + \Im^2(d(\omega))}} \quad \text{and} \quad \Phi_{\mathcal{G}}(\omega) = \arctan2\left(\frac{\Re(d(\omega))\Im(n(\omega)) - \Re(n(\omega))\Im(d(\omega))}{\Re(n(\omega))\Re(d(\omega)) + \Im(n(\omega))\Im(d(\omega))}\right), \quad \text{respectively.} \quad (50)$$

Moreover, by invoking the following trigonometric identities [39, Sect. 4.3–4.4]

$$\left. \begin{aligned} \sin(\alpha \pm \beta) &= \sin(\alpha)\cos(\beta) \pm \cos(\alpha)\sin(\beta), & \cos(\alpha \pm \beta) &= \cos(\alpha)\cos(\beta) \mp \sin(\alpha)\sin(\beta), \\ \sin(\arctan2\left(\frac{y}{x}\right)) &= \frac{y}{\sqrt{x^2 + y^2}} & \text{and} & & \cos(\arctan2\left(\frac{y}{x}\right)) &= \frac{x}{\sqrt{x^2 + y^2}}, \end{aligned} \right\} \quad (51)$$

the following expressions are obtained

$$\left. \begin{aligned} A_{\mathcal{G}}(\omega) \cos(\Phi_{\mathcal{G}}(\omega)) &\stackrel{(50),(51)}{=} \sqrt{\frac{\Re^2(n(\omega)) + \Im^2(n(\omega))}{\Re^2(d(\omega)) + \Im^2(d(\omega))}} \frac{\Re(n(\omega))\Re(d(\omega)) + \Im(n(\omega))\Im(d(\omega))}{\sqrt{(\Re(n(\omega))\Re(d(\omega)) + \Im(n(\omega))\Im(d(\omega)))^2 + (\Re(d(\omega))\Im(n(\omega)) - \Re(n(\omega))\Im(d(\omega)))^2}} \\ &= \frac{\Re(n(\omega))\Re(d(\omega)) + \Im(n(\omega))\Im(d(\omega))}{\Re^2(d(\omega)) + \Im^2(d(\omega))} \quad \text{and} \\ A_{\mathcal{G}}(\omega) \sin(\Phi_{\mathcal{G}}(\omega)) &\stackrel{(50),(51)}{=} \sqrt{\frac{\Re^2(n(\omega)) + \Im^2(n(\omega))}{\Re^2(d(\omega)) + \Im^2(d(\omega))}} \frac{\Re(d(\omega))\Im(n(\omega)) - \Re(n(\omega))\Im(d(\omega))}{\sqrt{(\Re(n(\omega))\Re(d(\omega)) + \Im(n(\omega))\Im(d(\omega)))^2 + (\Re(d(\omega))\Im(n(\omega)) - \Re(n(\omega))\Im(d(\omega)))^2}} \\ &= \frac{\Re(d(\omega))\Im(n(\omega)) - \Re(n(\omega))\Im(d(\omega))}{\Re^2(d(\omega)) + \Im^2(d(\omega))}. \end{aligned} \right\} \quad (52)$$

Second, let $t \in \mathbb{R}$ and $\nu, \omega > 0$ and consider the integral given by

$$\begin{aligned} \int_t^{t + \frac{2\pi}{\nu\omega}} \cos(\nu\omega\tau + \varphi_1) \cos(\nu\omega\tau + \varphi_2) d\tau &\stackrel{(51)}{=} \int_t^{t + \frac{2\pi}{\nu\omega}} \left(\cos^2(\nu\omega\tau) \cos(\varphi_1) \cos(\varphi_2) + \sin^2(\nu\omega\tau) \sin(\varphi_1) \sin(\varphi_2) \right) d\tau \\ &\quad - \int_t^{t + \frac{2\pi}{\nu\omega}} \sin(\nu\omega\tau) \cos(\nu\omega\tau) \sin(\varphi_1 + \varphi_2) d\tau. \end{aligned}$$

According to [26, p. 163f], it follows that

$$\int_t^{t + \frac{2\pi}{\nu\omega}} \cos(\nu\omega\tau + \varphi_1) \cos(\nu\omega\tau + \varphi_2) d\tau = \frac{\pi}{\nu\omega} \cos(\varphi_1) \cos(\varphi_2) + \frac{\pi}{\nu\omega} \sin(\varphi_1) \sin(\varphi_2) \stackrel{(51)}{=} \frac{\pi}{\nu\omega} \cos(\varphi_1 - \varphi_2). \quad (53)$$

2) *Steady-state analysis (amplitude and phase responses) of parallelized mSOGIs:* For constant $\hat{\omega} > 0$ and some $i \in \{1, \dots, n\}$, from Figures 1 and 3 (a) the transfer functions for the i -th in-phase signal ($\hat{\mathcal{Y}}_i(s)$), the i -th quadrature signal ($\hat{\mathcal{Q}}_i(s)$) and the overall estimation error ($\mathcal{E}_y(s)$) of the closed-loop observer system (13) are obtained as follows

$$\begin{aligned} \hat{\mathcal{Y}}_i(s) &:= \frac{\hat{y}_i(s)}{y(s)} = \frac{(k_i \nu_i \hat{\omega} s - g_i \nu_i^2 \hat{\omega}^2) \prod_{\substack{k=1 \\ k \neq i}}^n (s^2 + \nu_k^2 \hat{\omega}^2)}{\prod_{k=1}^n (s^2 + \nu_k^2 \hat{\omega}^2) - \sum_{k=1}^n g_k \nu_k^2 \hat{\omega}^2 \prod_{\substack{l=1 \\ l \neq k}}^n (s^2 + \nu_l^2 \hat{\omega}^2) + \sum_{k=1}^n k_k \nu_k \hat{\omega} s \prod_{\substack{l=1 \\ l \neq k}}^n (s^2 + \nu_l^2 \hat{\omega}^2)} \\ \hat{\mathcal{Q}}_i(s) &:= \frac{\hat{q}_i(s)}{y(s)} = \frac{(g_i \nu_i \hat{\omega} s + k_i \nu_i^2 \hat{\omega}^2) \prod_{\substack{k=1 \\ k \neq i}}^n (s^2 + \nu_k^2 \hat{\omega}^2)}{\prod_{k=1}^n (s^2 + \nu_k^2 \hat{\omega}^2) - \sum_{k=1}^n g_k \nu_k^2 \hat{\omega}^2 \prod_{\substack{l=1 \\ l \neq k}}^n (s^2 + \nu_l^2 \hat{\omega}^2) + \sum_{k=1}^n k_k \nu_k \hat{\omega} s \prod_{\substack{l=1 \\ l \neq k}}^n (s^2 + \nu_l^2 \hat{\omega}^2)} \\ \mathcal{E}_y(s) &:= \frac{e_y(s)}{y(s)} = \frac{\prod_{k=1}^n (s^2 + \nu_k^2 \hat{\omega}^2)}{\prod_{k=1}^n (s^2 + \nu_k^2 \hat{\omega}^2) - \sum_{k=1}^n g_k \nu_k^2 \hat{\omega}^2 \prod_{\substack{l=1 \\ l \neq k}}^n (s^2 + \nu_l^2 \hat{\omega}^2) + \sum_{k=1}^n k_k \nu_k \hat{\omega} s \prod_{\substack{l=1 \\ l \neq k}}^n (s^2 + \nu_l^2 \hat{\omega}^2)}. \end{aligned}$$

By invoking (50) from the preliminaries above and defining

$$\xi(\omega) := \sum_{k=1}^n k_k \nu_k \hat{\omega} \prod_{\substack{l=1 \\ l \neq k}}^n (\nu_l^2 \hat{\omega}^2 - \omega^2) \quad \text{and} \quad \zeta(\omega) := \prod_{k=1}^n (\nu_k^2 \hat{\omega}^2 - \omega^2) - \sum_{k=1}^n g_k \nu_k^2 \hat{\omega}^2 \prod_{\substack{l=1 \\ l \neq k}}^n (\nu_l^2 \hat{\omega}^2 - \omega^2), \quad (54)$$

their respective amplitude and phase responses can be computed as follows

$$\begin{aligned} A_{\hat{y}_i}(\omega) &= \nu_i \hat{\omega} \prod_{\substack{k=1 \\ k \neq i}}^n (\nu_k^2 \hat{\omega}^2 - \omega^2) \sqrt{\frac{k_i^2 \omega^2 + g_i^2 \nu_i^2 \hat{\omega}^2}{\left(\prod_{k=1}^n (\nu_k^2 \hat{\omega}^2 - \omega^2) - \sum_{k=1}^n g_k \nu_k^2 \hat{\omega}^2 \prod_{\substack{l=1 \\ l \neq k}}^n (\nu_l^2 \hat{\omega}^2 - \omega^2) \right)^2 + \left(\sum_{k=1}^n k_k \nu_k \hat{\omega} \prod_{\substack{l=1 \\ l \neq k}}^n (\nu_l^2 \hat{\omega}^2 - \omega^2) \right)^2}} \\ &\stackrel{(54)}{=} \nu_i \hat{\omega} \prod_{\substack{k=1 \\ k \neq i}}^n (\nu_k^2 \hat{\omega}^2 - \omega^2) \sqrt{\frac{k_i^2 \omega^2 + g_i^2 \nu_i^2 \hat{\omega}^2}{\zeta^2(\omega) + \xi^2(\omega)}}; \end{aligned} \quad (55)$$

$$\begin{aligned} \Phi_{\hat{y}_i}(\omega) &= \arctan 2 \left(\frac{k_i \omega \left(\prod_{k=1}^n (\nu_k^2 \hat{\omega}^2 - \omega^2) - \sum_{k=1}^n g_k \nu_k^2 \hat{\omega}^2 \prod_{\substack{l=1 \\ l \neq k}}^n (\nu_l^2 \hat{\omega}^2 - \omega^2) \right) + g_i \nu_i \hat{\omega} \sum_{k=1}^n k_k \nu_k \hat{\omega} \prod_{\substack{l=1 \\ l \neq k}}^n (\nu_l^2 \hat{\omega}^2 - \omega^2)}{k_i \omega \sum_{k=1}^n k_k \nu_k \hat{\omega} \prod_{\substack{l=1 \\ l \neq k}}^n (\nu_l^2 \hat{\omega}^2 - \omega^2) - g_i \nu_i \hat{\omega} \left(\prod_{k=1}^n (\nu_k^2 \hat{\omega}^2 - \omega^2) - \sum_{k=1}^n g_k \nu_k^2 \hat{\omega}^2 \prod_{\substack{l=1 \\ l \neq k}}^n (\nu_l^2 \hat{\omega}^2 - \omega^2) \right)} \right) \\ &\stackrel{(54)}{=} \arctan 2 \left(\frac{k_i \omega \zeta(\omega) + g_i \nu_i \hat{\omega} \xi(\omega)}{k_i \omega \xi(\omega) - g_i \nu_i \hat{\omega} \zeta(\omega)} \right); \end{aligned} \quad (56)$$

$$\begin{aligned} A_{\hat{Q}_i}(\omega) &= \nu_i \hat{\omega} \prod_{\substack{k=1 \\ k \neq i}}^n (\nu_k^2 \hat{\omega}^2 - \omega^2) \sqrt{\frac{g_i^2 \omega^2 + k_i^2 \nu_i^2 \hat{\omega}^2}{\left(\prod_{k=1}^n (\nu_k^2 \hat{\omega}^2 - \omega^2) - \sum_{k=1}^n g_k \nu_k^2 \hat{\omega}^2 \prod_{\substack{l=1 \\ l \neq k}}^n (\nu_l^2 \hat{\omega}^2 - \omega^2) \right)^2 + \left(\sum_{k=1}^n k_k \nu_k \hat{\omega} \prod_{\substack{l=1 \\ l \neq k}}^n (\nu_l^2 \hat{\omega}^2 - \omega^2) \right)^2}} \\ &\stackrel{(54)}{=} \nu_i \hat{\omega} \prod_{\substack{k=1 \\ k \neq i}}^n (\nu_k^2 \hat{\omega}^2 - \omega^2) \sqrt{\frac{g_i^2 \omega^2 + k_i^2 \nu_i^2 \hat{\omega}^2}{\zeta^2(\omega) + \xi^2(\omega)}}; \end{aligned} \quad (57)$$

$$\begin{aligned} \Phi_{\hat{Q}_i}(\omega) &= \arctan 2 \left(\frac{g_i \omega \left(\prod_{k=1}^n (\nu_k^2 \hat{\omega}^2 - \omega^2) - \sum_{k=1}^n g_k \nu_k^2 \hat{\omega}^2 \prod_{\substack{l=1 \\ l \neq k}}^n (\nu_l^2 \hat{\omega}^2 - \omega^2) \right) - k_i \nu_i \hat{\omega} \sum_{k=1}^n k_k \nu_k \hat{\omega} \prod_{\substack{l=1 \\ l \neq k}}^n (\nu_l^2 \hat{\omega}^2 - \omega^2)}{g_i \omega \sum_{k=1}^n k_k \nu_k \hat{\omega} \prod_{\substack{l=1 \\ l \neq k}}^n (\nu_l^2 \hat{\omega}^2 - \omega^2) + k_i \nu_i \hat{\omega} \left(\prod_{k=1}^n (\nu_k^2 \hat{\omega}^2 - \omega^2) - \sum_{k=1}^n g_k \nu_k^2 \hat{\omega}^2 \prod_{\substack{l=1 \\ l \neq k}}^n (\nu_l^2 \hat{\omega}^2 - \omega^2) \right)} \right) \\ &\stackrel{(54)}{=} \arctan 2 \left(\frac{g_i \omega \zeta(\omega) - k_i \nu_i \hat{\omega} \xi(\omega)}{g_i \omega \xi(\omega) + k_i \nu_i \hat{\omega} \zeta(\omega)} \right); \end{aligned} \quad (58)$$

$$A_{\mathcal{E}_y}(\omega) = \frac{\prod_{k=1}^n (\nu_k^2 \hat{\omega}^2 - \omega^2)}{\sqrt{\left(\prod_{k=1}^n (\nu_k^2 \hat{\omega}^2 - \omega^2) - \sum_{k=1}^n g_k \nu_k^2 \hat{\omega}^2 \prod_{\substack{l=1 \\ l \neq k}}^n (\nu_l^2 \hat{\omega}^2 - \omega^2) \right)^2 + \left(\sum_{k=1}^n k_k \nu_k \hat{\omega} \prod_{\substack{l=1 \\ l \neq k}}^n (\nu_l^2 \hat{\omega}^2 - \omega^2) \right)^2}} \stackrel{(54)}{=} \frac{\prod_{k=1}^n (\nu_k^2 \hat{\omega}^2 - \omega^2)}{\sqrt{\zeta^2(\omega) + \xi^2(\omega)}} \quad (59)$$

$$\Phi_{\mathcal{E}_y}(\omega) = \arctan 2 \left(\frac{-\sum_{k=1}^n k_k \nu_k \hat{\omega} \prod_{\substack{l=1 \\ l \neq k}}^n (\nu_l^2 \hat{\omega}^2 - \omega^2)}{\prod_{k=1}^n (\nu_k^2 \hat{\omega}^2 - \omega^2) - \sum_{k=1}^n g_k \nu_k^2 \hat{\omega}^2 \prod_{\substack{l=1 \\ l \neq k}}^n (\nu_l^2 \hat{\omega}^2 - \omega^2)} \right) \stackrel{(54)}{=} \arctan 2 \left(\frac{-\xi(\omega)}{\zeta(\omega)} \right). \quad (60)$$

Hence, for an input signal of the form

$$y(t) = \sum_{\nu \in \mathbb{H}_n} a_\nu \cos(\nu \omega t + \phi_{\nu,0}),$$

the estimated in-phase and quadrature signal and the overall error, in *quasi-steady state*, for all $i \in \{1, \dots, n\}$, are given by

$$\left. \begin{aligned} \hat{y}_i(t) &= \sum_{\nu \in \mathbb{H}_n} A_{\hat{y}_i}(\nu \omega) a_\nu \cos(\nu \omega t + \phi_{\nu,0} + \Phi_{\hat{y}_i}(\nu \omega)), \\ \hat{q}_i(t) &= \sum_{\nu \in \mathbb{H}_n} A_{\hat{Q}_i}(\nu \omega) a_\nu \cos(\nu \omega t + \phi_{\nu,0} + \Phi_{\hat{Q}_i}(\nu \omega)), \\ e_y(t) &= \sum_{\nu \in \mathbb{H}_n} A_{\mathcal{E}_y}(\nu \omega) a_\nu \cos(\nu \omega t + \phi_{\nu,0} + \Phi_{\mathcal{E}_y}(\nu \omega)), \end{aligned} \right\} \quad \text{and} \quad (61)$$

respectively.

3) *Sign-correct adaption law*: Now, the main result of this appendix can be presented.

Proposition A.6 (Sign-correct adaption over one period). *Let $\omega > 0$ and $T_i := \frac{2\pi}{\nu_i \omega}$ for $\nu_i \in \mathbb{H}_n$ and $i \in \{1, \dots, n\}$. Consider system (29) with $\widehat{\omega} > 0$ and introduce the integral*

$$\int_t^{t+T_i} e_{i,\infty}(\tau) \boldsymbol{\lambda}^\top \widehat{\boldsymbol{x}}_{i,i,\infty}(\tau) d\tau \quad (62)$$

where $e_{i,\infty}$ is the i -th error component and $\widehat{\boldsymbol{x}}_{i,i,\infty}$ is the i -th component of the i -th state vector in quasi-steady state (indicated by the subscript " ∞ "). Then, the following holds

$$\forall \boldsymbol{\lambda} \in \mathbb{R}^{2n} \in \left\{ \boldsymbol{\alpha} \left| \boldsymbol{l}^\top \underbrace{\text{blockdiag}(\mathbf{O}_{2 \times 2}, \dots, \overline{\mathbf{J}}, \dots, \mathbf{O}_{2 \times 2})}_{=:\mathbf{J}_i} \boldsymbol{\alpha} < 0 \right. \right\} : \int_t^{t+T_i} e_{i,\infty}(\tau) \boldsymbol{\lambda}^\top \widehat{\boldsymbol{x}}_{i,i,\infty}(\tau) d\tau \begin{cases} > 0, & \widehat{\omega} < \omega \\ = 0, & \widehat{\omega} = \omega \\ < 0, & \widehat{\omega} > \omega. \end{cases} \quad (63)$$

Moreover, if $\boldsymbol{\lambda} = \mathbf{J}_i^{-1} \mathbf{l}$, then the integral (62) over one period T_i attains its maximal (or minimal, resp.) value and the phases of $e_{i,\infty}(t)$ and $\widehat{\boldsymbol{x}}_{i,i,\infty}(t)$ are identical.

Proof. Define $\boldsymbol{\lambda} := (0, 0, \dots, \underbrace{\lambda_{y,i}, \lambda_{q,i}}_{=:\boldsymbol{\lambda}_i^\top \in \mathbb{R}^2}, \dots, 0, 0)^\top \in \mathbb{R}^{2n}$ and observe that

$$\boldsymbol{\lambda}_i^\top \widehat{\boldsymbol{x}}_{i,i,\infty}(t) \stackrel{(61)}{=} \lambda_{q,i} A_{\widehat{\mathcal{Q}}_i}(\nu_i \omega) a_{\nu_i} \cos(\nu_i \omega t + \Phi_{\widehat{\mathcal{Q}}_i}(\nu_i \omega)) + \lambda_{y,i} A_{\widehat{\mathcal{Y}}_i}(\nu_i \omega) a_{\nu_i} \cos(\nu_i \omega t + \Phi_{\widehat{\mathcal{Y}}_i}(\nu_i \omega)). \quad (64)$$

By invoking the trigonometric identities [26, p. 125]

$$\left. \begin{aligned} \sum_{i=1}^n a_i \cos(\alpha_i) &= \sqrt{\sum_{i=1}^n \sum_{j=1}^n a_i a_j \cdot \cos(\alpha_i - \alpha_j) \cos\left(\alpha_1 + \arctan 2\left(\frac{\sum_{i=1}^n a_i \sin(\alpha_i - \alpha_1)}{\sum_{i=1}^n a_i \cos(\alpha_i - \alpha_1)}\right)\right)} \quad \text{and} \\ \arctan 2\left(\frac{y_1}{x_1}\right) + \arctan 2\left(\frac{y_2}{x_2}\right) &= \arctan 2\left(\frac{\frac{y_1}{x_1} + \frac{y_2}{x_2}}{1 - \frac{y_1 y_2}{x_1 x_2}}\right), \end{aligned} \right\} \quad (65)$$

it follows

$$\begin{aligned} \boldsymbol{\lambda}_i^\top \widehat{\boldsymbol{x}}_{i,i,\infty}(t) &\stackrel{(64),(65)}{=} \sqrt{\lambda_{q,i}^2 A_{\widehat{\mathcal{Q}}_i}^2(\nu_i \omega) a_{\nu_i}^2 + \lambda_{y,i}^2 A_{\widehat{\mathcal{Y}}_i}^2(\nu_i \omega) a_{\nu_i}^2 + 2\lambda_{q,i} \lambda_{y,i} A_{\widehat{\mathcal{Q}}_i}(\nu_i \omega) A_{\widehat{\mathcal{Y}}_i}(\nu_i \omega) a_{\nu_i}^2 \cos(\Phi_{\widehat{\mathcal{Q}}_i}(\nu_i \omega) - \Phi_{\widehat{\mathcal{Y}}_i}(\nu_i \omega))} \\ &\quad \cdot \cos\left(\nu_i \omega t + \Phi_{\widehat{\mathcal{Q}}_i}(\nu_i \omega) + \arctan 2\left(\frac{\lambda_{y,i} A_{\widehat{\mathcal{Y}}_i}(\nu_i \omega) a_{\nu_i} \sin(\Phi_{\widehat{\mathcal{Y}}_i}(\nu_i \omega) - \Phi_{\widehat{\mathcal{Q}}_i}(\nu_i \omega))}{\lambda_{q,i} A_{\widehat{\mathcal{Q}}_i}(\nu_i \omega) a_{\nu_i} + \lambda_{y,i} A_{\widehat{\mathcal{Y}}_i}(\nu_i \omega) a_{\nu_i} \cos(\Phi_{\widehat{\mathcal{Y}}_i}(\nu_i \omega) - \Phi_{\widehat{\mathcal{Q}}_i}(\nu_i \omega))}\right)\right) \\ &\stackrel{(51),(52)}{=} a_{\nu_i} \frac{\nu_i^2 \widehat{\omega} \prod_{\substack{k=1 \\ k \neq i}}^n (\nu_k^2 \widehat{\omega}^2 - \nu_i^2 \omega^2)}{\sqrt{\zeta^2(\nu_i \omega) + \xi^2(\nu_i \omega)}} \sqrt{\lambda_{q,i}^2 (g_i^2 \omega^2 + k_i^2 \widehat{\omega}^2) + \lambda_{y,i}^2 (k_i^2 \omega^2 + g_i^2 \widehat{\omega}^2) + 2\lambda_{y,i} \lambda_{q,i} k_i g_i (\omega^2 - \widehat{\omega}^2)} \\ &\quad \cdot \cos\left(\nu_i \omega t + \arctan 2\left(\frac{g_i \omega \zeta(\nu_i \omega) - k_i \widehat{\omega} \xi(\nu_i \omega)}{g_i \omega \xi(\nu_i \omega) + k_i \widehat{\omega} \zeta(\nu_i \omega)}\right) + \arctan 2\left(\frac{\lambda_{y,i} \frac{(k_i^2 + g_i^2) \widehat{\omega} \omega}{\sqrt{(g_i^2 \omega^2 + k_i^2 \widehat{\omega}^2)}}}{\lambda_{q,i} \sqrt{g_i^2 \omega^2 + k_i^2 \widehat{\omega}^2} + \lambda_{y,i} \frac{k_i g_i (\omega^2 - \widehat{\omega}^2)}{\sqrt{(g_i^2 \omega^2 + k_i^2 \widehat{\omega}^2)}}}\right)\right) \\ &\stackrel{(65)}{=} a_{\nu_i} \frac{\nu_i^2 \widehat{\omega} \prod_{\substack{k=1 \\ k \neq i}}^n (\nu_k^2 \widehat{\omega}^2 - \nu_i^2 \omega^2)}{\sqrt{\zeta^2(\nu_i \omega) + \xi^2(\nu_i \omega)}} \sqrt{(\lambda_{y,i} k_i + \lambda_{q,i} g_i)^2 \omega^2 + (\lambda_{y,i} g_i - \lambda_{q,i} k_i)^2 \widehat{\omega}^2} \\ &\quad \cdot \cos\left(\nu_i \omega t + \arctan 2\left(\frac{\frac{g_i \omega \zeta(\nu_i \omega) - k_i \widehat{\omega} \xi(\nu_i \omega)}{g_i \omega \xi(\nu_i \omega) + k_i \widehat{\omega} \zeta(\nu_i \omega)} + \frac{\lambda_{y,i} \widehat{\omega} \omega (k_i^2 + g_i^2)}{\lambda_{q,i} (g_i^2 \omega^2 + k_i^2 \widehat{\omega}^2) + \lambda_{y,i} (k_i g_i (\omega^2 - \widehat{\omega}^2))}}{1 - \frac{g_i \omega \zeta(\nu_i \omega) - k_i \widehat{\omega} \xi(\nu_i \omega)}{g_i \omega \xi(\nu_i \omega) + k_i \widehat{\omega} \zeta(\nu_i \omega)} \frac{\lambda_{y,i} \widehat{\omega} \omega (k_i^2 + g_i^2)}{\lambda_{q,i} (g_i^2 \omega^2 + k_i^2 \widehat{\omega}^2) + \lambda_{y,i} (k_i g_i (\omega^2 - \widehat{\omega}^2))}}\right)\right) \\ &= a_{\nu_i} \frac{\nu_i^2 \widehat{\omega} \prod_{\substack{k=1 \\ k \neq i}}^n (\nu_k^2 \widehat{\omega}^2 - \nu_i^2 \omega^2)}{\sqrt{\zeta^2(\nu_i \omega) + \xi^2(\nu_i \omega)}} \sqrt{(\lambda_{y,i} k_i + \lambda_{q,i} g_i)^2 \omega^2 + (\lambda_{y,i} g_i - \lambda_{q,i} k_i)^2 \widehat{\omega}^2} \\ &\quad \cdot \cos\left(\nu_i \omega t + \arctan 2\left(\frac{\lambda_{q,i} (g_i \omega \zeta(\nu_i \omega) - k_i \widehat{\omega} \xi(\nu_i \omega)) + \lambda_{y,i} (g_i \widehat{\omega} \xi(\nu_i \omega) + k_i \omega \zeta(\nu_i \omega))}{\lambda_{q,i} (g_i \omega \xi(\nu_i \omega) + k_i \widehat{\omega} \zeta(\nu_i \omega)) + \lambda_{y,i} (k_i \omega \xi(\nu_i \omega) - g_i \widehat{\omega} \zeta(\nu_i \omega))}\right)\right). \quad (66) \end{aligned}$$

Now, multiplying $\lambda_i^\top \widehat{\mathbf{x}}_{i,i,\infty}(t)$ with $e_{i,\infty}(t)$ yields

$$e_{i,\infty}(t) \lambda_i^\top \widehat{\mathbf{x}}_{i,i,\infty}(t) \stackrel{(59),(60),(66)}{=} a_{\nu_i}^2 \frac{\nu_i^4 \widehat{\omega} \prod_{\substack{k=1 \\ k \neq i}}^n (\nu_k^2 \widehat{\omega}^2 - \nu_i^2 \omega^2)^2 (\widehat{\omega}^2 - \omega^2)}{\zeta^2(\nu_i \omega) + \xi^2(\nu_i \omega)} \sqrt{(\lambda_{y,i} k_i + \lambda_{q,i} g_i)^2 \omega^2 + (\lambda_{y,i} g_i - \lambda_{q,i} k_i)^2 \widehat{\omega}^2} \cos\left(\nu_i \omega \tau + \arctan 2\left(\frac{-\xi(\nu_i \omega)}{\zeta(\nu_i \omega)}\right)\right) \cos\left(\nu_i \omega \tau + \arctan 2\left(\frac{\lambda_{q,i}(g_i \omega \zeta(\nu_i \omega) - k_i \widehat{\omega} \xi(\nu_i \omega)) + \lambda_{y,i}(g_i \widehat{\omega} \xi(\nu_i \omega) + k_i \omega \zeta(\nu_i \omega))}{\lambda_{q,i}(g_i \omega \xi(\nu_i \omega) + k_i \widehat{\omega} \zeta(\nu_i \omega)) + \lambda_{y,i}(k_i \omega \xi(\nu_i \omega) - g_i \widehat{\omega} \zeta(\nu_i \omega))}\right)\right). \quad (67)$$

Solving the integral (62) over one period $T_i = \frac{2\pi}{\nu_i \omega}$ gives

$$\begin{aligned} & \int_t^{t+\frac{2\pi}{\nu_i \omega}} e_{i,\infty}(\tau) \lambda_i^\top \widehat{\mathbf{x}}_{i,i,\infty}(\tau) d\tau \stackrel{(67)}{=} a_{\nu_i}^2 \frac{\nu_i^4 \widehat{\omega} \prod_{\substack{k=1 \\ k \neq i}}^n (\nu_k^2 \widehat{\omega}^2 - \nu_i^2 \omega^2)^2 (\widehat{\omega}^2 - \omega^2)}{\zeta^2(\nu_i \omega) + \xi^2(\nu_i \omega)} \sqrt{(\lambda_{y,i} k_i + \lambda_{q,i} g_i)^2 \omega^2 + (\lambda_{y,i} g_i - \lambda_{q,i} k_i)^2 \widehat{\omega}^2} \\ & \int_t^{t+\frac{2\pi}{\nu_i \omega}} \cos\left(\nu_i \omega \tau + \arctan 2\left(\frac{-\xi(\nu_i \omega)}{\zeta(\nu_i \omega)}\right)\right) \cos\left(\nu_i \omega \tau + \arctan 2\left(\frac{\lambda_{q,i}(g_i \omega \zeta(\nu_i \omega) - k_i \widehat{\omega} \xi(\nu_i \omega)) + \lambda_{y,i}(g_i \widehat{\omega} \xi(\nu_i \omega) + k_i \omega \zeta(\nu_i \omega))}{\lambda_{q,i}(g_i \omega \xi(\nu_i \omega) + k_i \widehat{\omega} \zeta(\nu_i \omega)) + \lambda_{y,i}(k_i \omega \xi(\nu_i \omega) - g_i \widehat{\omega} \zeta(\nu_i \omega))}\right)\right) d\tau \\ & \stackrel{(53)}{=} a_{\nu_i}^2 \frac{\nu_i^4 \widehat{\omega} \prod_{\substack{k=1 \\ k \neq i}}^n (\nu_k^2 \widehat{\omega}^2 - \nu_i^2 \omega^2)^2 (\widehat{\omega}^2 - \omega^2)}{\zeta^2(\nu_i \omega) + \xi^2(\nu_i \omega)} \sqrt{(\lambda_{y,i} g_i - \lambda_{q,i} k_i)^2 \widehat{\omega}^2 + (\lambda_{y,i} k_i + \lambda_{q,i} g_i)^2 \omega^2} \\ & \frac{\pi}{\nu_i \omega} \cos\left(\arctan 2\left(\frac{-\xi(\nu_i \omega)}{\zeta(\nu_i \omega)}\right) - \arctan 2\left(\frac{\lambda_{q,i}(g_i \omega \zeta(\nu_i \omega) - k_i \widehat{\omega} \xi(\nu_i \omega)) + \lambda_{y,i}(g_i \widehat{\omega} \xi(\nu_i \omega) + k_i \omega \zeta(\nu_i \omega))}{\lambda_{q,i}(g_i \omega \xi(\nu_i \omega) + k_i \widehat{\omega} \zeta(\nu_i \omega)) + \lambda_{y,i}(k_i \omega \xi(\nu_i \omega) - g_i \widehat{\omega} \zeta(\nu_i \omega))}\right)\right) \\ & \stackrel{(65)}{=} a_{\nu_i}^2 \frac{\pi \nu_i^3 \widehat{\omega} \prod_{\substack{k=1 \\ k \neq i}}^n (\nu_k^2 \widehat{\omega}^2 - \nu_i^2 \omega^2)^2 (\widehat{\omega}^2 - \omega^2)}{\omega (\zeta^2(\nu_i \omega) + \xi^2(\nu_i \omega))} \sqrt{(\lambda_{y,i} g_i - \lambda_{q,i} k_i)^2 \widehat{\omega}^2 + (\lambda_{y,i} k_i + \lambda_{q,i} g_i)^2 \omega^2} \cos\left(\arctan 2\left(\frac{-(\lambda_{q,i} g_i + \lambda_{y,i} k_i) \omega}{(\lambda_{q,i} k_i - \lambda_{y,i} g_i) \widehat{\omega}}\right)\right) \\ & \stackrel{(51)}{=} a_{\nu_i}^2 \frac{\pi \nu_i^3 \widehat{\omega}^2 \prod_{\substack{k=1 \\ k \neq i}}^n (\nu_k^2 \widehat{\omega}^2 - \nu_i^2 \omega^2)^2 (\widehat{\omega}^2 - \omega^2)}{\omega (\zeta^2(\nu_i \omega) + \xi^2(\nu_i \omega))} (\lambda_{q,i} k_i - \lambda_{y,i} g_i) = a_{\nu_i}^2 \frac{\pi \nu_i^2 \widehat{\omega}^2 \prod_{\substack{k=1 \\ k \neq i}}^n (\nu_k^2 \widehat{\omega}^2 - \nu_i^2 \omega^2)^2 (\omega^2 - \widehat{\omega}^2)}{\omega (\zeta^2(\nu_i \omega) + \xi^2(\nu_i \omega))} \mathbf{l}^\top \mathbf{J}_i \boldsymbol{\lambda}. \quad (68) \end{aligned}$$

Since $\omega > 0$, observe that only $\omega^2 - \widehat{\omega}^2$ can change its sign in (68); all other terms of the nominator and denominator are positive. Hence, only for $\mathbf{l}^\top \mathbf{J}_i \boldsymbol{\lambda} > 0$, the following condition is satisfied

$$\forall \boldsymbol{\lambda} \in \left\{ \boldsymbol{\alpha} \in \mathbb{R}^{2n} \mid \mathbf{l}^\top \mathbf{J}_i \boldsymbol{\lambda} > 0 \right\} : \int_t^{t+T_i} e_{i,\infty}(\tau) \boldsymbol{\lambda}^\top \widehat{\mathbf{x}}_{i,i,\infty}(\tau) d\tau \begin{cases} > 0, & \widehat{\omega} < \omega \\ = 0, & \widehat{\omega} = \omega \\ < 0, & \widehat{\omega} > \omega, \end{cases}$$

which proves assertion (63). To optimize (68) (to obtain maximal or minimal value), $\boldsymbol{\lambda} = \mathbf{J}_i^{-1} \mathbf{l}$ must hold, since

$$\mathbf{l}^\top \mathbf{J}_i \boldsymbol{\lambda} = \mathbf{l}^\top \mathbf{l} = k_i^2 + g_i^2.$$

Moreover, for $\boldsymbol{\lambda} = \mathbf{J}_i^{-1} \mathbf{l}$, the phase is given by

$$\Phi_{\boldsymbol{\lambda}^\top \widehat{\mathbf{x}}_{i,i,\infty}(t)} \stackrel{(66)}{=} \arctan 2\left(\frac{\lambda_{q,i}(g_i \omega \zeta(\nu_i \omega) - k_i \widehat{\omega} \xi(\nu_i \omega)) + \lambda_{y,i}(g_i \widehat{\omega} \xi(\nu_i \omega) + k_i \omega \zeta(\nu_i \omega))}{\lambda_{q,i}(g_i \omega \xi(\nu_i \omega) + k_i \widehat{\omega} \zeta(\nu_i \omega)) + \lambda_{y,i}(k_i \omega \xi(\nu_i \omega) - g_i \widehat{\omega} \zeta(\nu_i \omega))}\right) \stackrel{\boldsymbol{\lambda} = \mathbf{J}_i^{-1} \mathbf{l}}{=} \arctan 2\left(\frac{-\xi(\nu_i \omega)}{\zeta(\nu_i \omega)}\right),$$

which is identical to $\Phi_{\mathcal{E}_y}(\nu_i \omega)$ in (60). This completes the proof. \square

Concluding, the choice $\boldsymbol{\lambda} = \mathbf{J}_i^{-1} \mathbf{l}$ gives the optimal choice for the adaption law (26) of the modified Frequency Locked Loop: It guarantees sign-correct (phase-correct) and optimal adaption, in the sense that the maximal or minimal value of $e_{i,\infty}(t) \boldsymbol{\lambda}^\top \widehat{\mathbf{x}}_{i,i,\infty}(t)$ is fed to the adaption law.

REFERENCES

- [1] C. M. Hackl and M. Landerer, "Modified second-order generalized integrators with modified frequency locked loop for fast harmonics estimation of distorted single-phase signals," *IEEE Transactions on Power Electronics*, 2019.
- [2] F. Milano, F. Dörfler, G. Hug, D. J. Hill, and G. Verbič, "Foundations and challenges of low-inertia systems (invited paper)," in *2018 Power Systems Computation Conference (PSCC)*, pp. 1–25, June 2018.
- [3] P. Rodríguez, A. Luna, M. Ciobotaru, R. Teodorescu, and F. Blaabjerg, "Advanced grid synchronization system for power converters under unbalanced and distorted operating conditions," in *IECON 2006 - 32nd Annual Conference on IEEE Industrial Electronics*, pp. 5173–5178, Nov 2006.
- [4] M. Mojiri, M. Karimi-Ghartemani, and A. Bakhshai, "Time-domain signal analysis using adaptive notch filter," *IEEE Transactions on Signal Processing*, vol. 55, pp. 85–93, Jan 2007.
- [5] R. S. R. Chilipi, N. A. Sayari, K. H. A. Hosani, and A. R. Beig, "Adaptive notch filter-based multipurpose control scheme for grid-interfaced three-phase four-wire DG inverter," *IEEE Transactions on Industry Applications*, vol. 53, pp. 4015–4027, July 2017.
- [6] G. Fedele, A. Ferrise, and D. Frascino, "Structural properties of the SOGI system for parameters estimation of a biased sinusoid," in *2010 9th International Conference on Environment and Electrical Engineering*, pp. 438–441, May 2010.
- [7] P. Rodríguez, A. Luna, I. Candela, R. Mujal, R. Teodorescu, and F. Blaabjerg, "Multiresonant frequency-locked loop for grid synchronization of power converters under distorted grid conditions," *IEEE Transactions on Industrial Electronics*, vol. 58, pp. 127–138, Jan 2011.
- [8] F. Muzi and M. Barbati, "A real-time harmonic monitoring aimed at improving smart grid power quality," in *2011 IEEE International Conference on Smart Measurements of Future Grids (SMFG) Proceedings*, pp. 95–100, Nov 2011.
- [9] Z. Luo, M. Kaye, C. Diduch, and L. Chang, "Frequency measurement using a frequency locked loop," in *2011 IEEE Energy Conversion Congress and Exposition*, pp. 917–921, Sep. 2011.
- [10] J. Park, D. Lee, and T. L. Van, "Advanced single-phase SOGI-FLL using self-tuning gain based on fuzzy logic," in *2013 IEEE ECCE Asia Downunder*, pp. 1282–1288, June 2013.
- [11] A. Kulkarni and V. John, "A novel design method for SOGI-PLL for minimum settling time and low unit vector distortion," in *IECON 2013 - 39th Annual Conference of the IEEE Industrial Electronics Society*, pp. 274–279, Nov 2013.
- [12] S. K. Panda and T. K. Dash, "An improved method of frequency detection for grid synchronization of DG systems during grid abnormalities," in *2014 International Conference on Circuits, Power and Computing Technologies [ICCPCT-2014]*, pp. 153–157, March 2014.
- [13] P. Cossutta, S. Raffo, A. Cao, F. Ditaranto, M. P. Aguirre, and M. I. Valla, "High speed single phase SOGI-PLL with high resolution implementation on an FPGA," in *2015 IEEE 24th International Symposium on Industrial Electronics (ISIE)*, pp. 1004–1009, June 2015.
- [14] Z. Xin, R. Zhao, P. K. Mattavelli, P. C. Loh, and F. Blaabjerg, "Re-investigation of generalized integrator based filters from a first-order-system perspective," *IEEE Access*, vol. 4, pp. 7131–7144, 2016.
- [15] K. R. Patil and H. H. Patel, "Modified dual second-order generalised integrator FLL for synchronization of a distributed generator to a weak grid," in *2016 IEEE 16th International Conference on Environment and Electrical Engineering (EEEIC)*, Institute of Electrical and Electronics Engineers (IEEE), Jun 2016.
- [16] S. Golestan, J. M. Guerrero, and J. C. Vasquez, "A robust and fast synchronization technique for adverse grid conditions," *IEEE Transactions on Industrial Electronics*, pp. 1–1, 2016.
- [17] J. Matas, H. Martin, J. de la Hoz, A. Abusorrah, Y. A. Al-Turki, and M. Al-Hindawi, "A family of gradient descent grid frequency estimators for the sogi filter," *IEEE Transactions on Power Electronics*, vol. PP, no. 99, pp. 1–1, 2017.
- [18] I. Ralev, A. Klein-Hessling, B. Pariti, and R. W. D. Doncker, "Adopting a SOGI filter for flux-linkage based rotor position sensing of switched reluctance machines," in *2017 IEEE International Electric Machines and Drives Conference (IEMDC)*, pp. 1–7, May 2017.
- [19] F. Xiao, L. Dong, L. Li, and X. Liao, "A frequency-fixed SOGI-based PLL for single-phase grid-connected converters," *IEEE Transactions on Power Electronics*, vol. 32, pp. 1713–1719, March 2017.
- [20] H. Yi, X. Wang, F. Blaabjerg, and F. Zhuo, "Impedance analysis of SOGI-FLL-based grid synchronization," *IEEE Transactions on Power Electronics*, vol. 32, pp. 7409–7413, Oct 2017.
- [21] S. Golestan, S. Y. Mousazadeh, J. M. Guerrero, and J. C. Vasquez, "A critical examination of frequency-fixed second-order generalized integrator-based phase-locked loops," *IEEE Transactions on Power Electronics*, vol. 32, pp. 6666–6672, Sep. 2017.
- [22] S. Golestan, J. M. Guerrero, and J. C. Vasquez, "Three-phase PLLs: A review of recent advances," *IEEE Transactions on Power Electronics*, vol. 32, pp. 1894–1907, Mar 2017.
- [23] Z. Dai, Z. Zhang, Y. Yang, F. Blaabjerg, Y. Huangfu, and J. Zhang, "A fixed-length transfer delay-based adaptive frequency locked loop for single-phase systems," *IEEE Transactions on Power Electronics*, pp. 1–1, 2018.
- [24] A. E. Karkevandi and M. J. Daryani, "Frequency estimation with antiwindup to improve sogi filter transient response to voltage sags," in *2018 6th International Istanbul Smart Grids and Cities Congress and Fair (ICSG)*, pp. 188–192, April 2018.
- [25] X. He, H. Geng, and G. Yang, "Reinvestigation of single-phase FLLs," *IEEE Access*, vol. 7, pp. 13178–13188, 2019.
- [26] L. Råde and B. Westergren, *Springers Mathematische Formeln: Taschenbuch für Ingenieure, Naturwissenschaftler, Informatiker, Wirtschaftswissenschaftler*. Springer Berlin Heidelberg, 2000.
- [27] R. Teodorescu, M. Liserre, and P. Rodríguez, *Grid Converters for Photovoltaic and Wind Power Systems*. Chichester, United Kingdom: John Wiley & Sons, Ltd., 2011.
- [28] S. Reza, M. Ciobotaru, and V. G. Agelidis, "Accurate estimation of single-phase grid voltage fundamental amplitude and frequency by using a frequency adaptive linear kalman filter," *IEEE Journal of Emerging and Selected Topics in Power Electronics*, vol. 4, pp. 1226–1235, Dec 2016.
- [29] M. S. Reza, M. Ciobotaru, and V. G. Agelidis, "Accurate estimation of single-phase grid voltage parameters under distorted conditions," *IEEE Transactions on Power Delivery*, vol. 29, pp. 1138–1146, June 2014.
- [30] H. Ahmed, S. Amamra, and M. H. Bierhoff, "Frequency-locked loop based estimation of single-phase grid voltage parameters," *IEEE Transactions on Industrial Electronics*, pp. 1–1, 2018.
- [31] D. Hinrichsen and A. Pritchard, *Mathematical Systems Theory I — Modelling, State Space Analysis, Stability and Robustness*. No. 48 in Texts in Applied Mathematics, Berlin: Springer-Verlag, 2005.
- [32] W. M. Wonham, *Linear Multivariable Control: A Geometric Approach*. No. 10 in Applications of Mathematics, Berlin: Springer-Verlag, 3 ed., 1985.
- [33] C. M. Hackl, *Non-identifier based adaptive control in mechatronics: Theory and Application*. No. 466 in Lecture Notes in Control and Information Sciences, Berlin: Springer International Publishing, 2017.
- [34] W. Rugh, *Linear System Theory*. Upper Saddle River, New Jersey: Prentice Hall International Inc., 2 ed., 1996.
- [35] D. S. Bernstein, *Matrix Mathematics — Theory, Facts, and Formulas with Application to Linear System Theory*. Princeton and Oxford: Princeton University Press, 2 ed., 2009.
- [36] H. K. Khalil, *Nonlinear Systems*. Upper Saddle River, New Jersey: Prentice-Hall International Inc., 3 ed., 2002.
- [37] B. A. Francis and W. M. Wonham, "The internal model principle of control theory," *Automatica*, vol. 12, no. 5, pp. 457–465, 1976.
- [38] A. A. Agrachev, A. S. Morse, E. D. Sontag, H. J. Sussmann, and V. I. Utkin, *Nonlinear and Optimal Control Theory*, vol. 1932 of *Lecture Notes in Mathematics*. Springer Berlin Heidelberg, 2008.
- [39] D. S., M. Abramowitz, and I. A. Stegun, *Handbook of Mathematical Functions With Formulas, Graphs and Mathematical Tables*. No. 55 in Applied Mathematics Series, Washington: National Bureau of Standards, 10 ed., 1964.